

Article

Transcriptomics and Metabolomics of Reactive Oxygen Species Modulation in Near-Null Magnetic Field-Induced *Arabidopsis thaliana*

Ambra S. Parmagnani [†] , Giuseppe Mannino [†]  and Massimo E. Maffei ^{*†} 

Department of Life Sciences and Systems Biology, University of Turin, Via G. Quarello 15/a, 10135 Turin, Italy

* Correspondence: massimo.maffei@unito.it; Tel.: +39-011-670-5967

† These authors contributed equally to this work.

Abstract: The geomagnetic field (GMF) is a natural component of Earth's biosphere. GMF reduction to near-null values (NNMF) induces gene expression modulation that generates biomolecular, morphological, and developmental changes. Here, we evaluate the effect of NNMF on gene expression and reactive oxygen species (ROS) production in time-course experiments on *Arabidopsis thaliana*. Plants exposed to NNMF in a triaxial Helmholtz coils system were sampled from 10 min to 96 h to evaluate differentially expressed genes (DEGs) of oxidative stress responses by gene microarray. In 24–96 h developing stages, H₂O₂ and polyphenols were also analyzed from roots and shoots. A total of 194 DEGs involved in oxidative reactions were selected, many of which showed a fold change $\geq \pm 2$ in at least one timing point. Heatmap clustering showed DEGs both between roots/shoots and among the different time points. NNMF induced a lower H₂O₂ than GMF, in agreement with the expression of ROS-related genes. Forty-four polyphenols were identified, the content of which progressively decreased during NNMF exposition time. The comparison between polyphenols content and DEGs showed overlapping patterns. These results indicate that GMF reduction induces metabolomic and transcriptomic modulation of ROS-scavenging enzymes and H₂O₂ production in *A. thaliana*, which is paralleled by the regulation of antioxidant polyphenols.

Keywords: reduction of geomagnetic field; gene expression; metabolomics; flavonoids; isoflavonoids; hydrogen peroxide



Citation: Parmagnani, A.S.; Mannino, G.; Maffei, M.E. Transcriptomics and Metabolomics of Reactive Oxygen Species Modulation in Near-Null Magnetic Field-Induced *Arabidopsis thaliana*. *Biomolecules* **2022**, *12*, 1824. <https://doi.org/10.3390/biom12121824>

Academic Editor: Georgia Ntatsi

Received: 18 November 2022

Accepted: 4 December 2022

Published: 6 December 2022

Publisher's Note: MDPI stays neutral with regard to jurisdictional claims in published maps and institutional affiliations.



Copyright: © 2022 by the authors. Licensee MDPI, Basel, Switzerland. This article is an open access article distributed under the terms and conditions of the Creative Commons Attribution (CC BY) license (<https://creativecommons.org/licenses/by/4.0/>).

1. Introduction

A growing body of evidence indicates that plants react to varying magnetic field (MF) fluxes at values both below and above the geomagnetic field (GMF) [1–3]. Reduction of the GMF (20–60 μ T) to Near Null Magnetic Field (NNMF, about 30 nT) has been shown to influence many plant biological processes [4,5].

In living systems, four different mechanisms of magnetoperception have been described: (i) the radical pairs mechanism (i.e., magnetically sensitive chemical intermediates that are formed by photoexcitation of cryptochrome [6,7]), which is present in animals [8], humans [9] and plants [10]; (ii) the presence of MF sensory receptors described in magnetotactic bacteria [11]; (iii) the presence of electroreceptors in elasmobranch animals [12] and; (iv) the biocompass model based on MagR/Cry complex [13]. Among the four possible mechanisms of magnetoreception, at least two (the radical pair mechanism (RPM) of chemical magnetosensing and the MagR/Cry biocompass) adequately explain the alterations in the MF by the rates of redox reactions and subsequently altered concentrations of free radicals and reactive oxygen species (ROS) observed in plants [10,14–18].

Cryptochrome (Cry) modulates ROS in response to weak MFs through altering the rate of redox reactions in the presence of a MF [10,19]. This phenomenon affects the cellular ROS production (in the nucleus and cytosol, and possibly also in other organelles as well) and is proposed to be similar in both plants and animals [3,18]. This mechanism perfectly predicts

an effect on cellular ROS signaling pathways; therefore, this hypothesis explains the ROS-related modulation of gene expression in response to MFs that has been observed in recent studies [20]. MF type/intensity/frequency, exposure time and assay time point, as well as different biological samples have been demonstrated to induce different ROS levels [21].

It is assumed that the singlet recombination of the $\text{FADH}^\bullet/\text{O}_2^{\bullet-}$ -RPM produces hydrogen peroxide (H_2O_2), possibly via the C4a-hydroperoxy-flavin, and that C^\bullet re-oxidizes FADH^\bullet to FAD [22]. It has also been proposed that that $\text{O}_2^{\bullet-}$ and H_2O_2 production in some metabolic processes occur through singlet–triplet modulation of semiquinone flavin (FADH^\bullet) enzymes and $\text{O}_2^{\bullet-}$ spin-correlated radical pairs [23].

Therefore, the aim of this work was to explore the transcriptomics and metabolomics of ROS production/metabolism by time-course gene expression analysis in both roots and shoots and to evaluate the production of both ROS and scavenging biomolecules in *Arabidopsis thaliana* plants exposed to NNMF conditions.

2. Materials and Methods

2.1. Plant Materials and Growth Conditions

Arabidopsis thaliana ecotype Columbia-0 (Col-0) wild-type (WT) seeds were surface-sterilized with 70% (*v/v*) ethanol for 15 min and then quickly washed with 100% (*v/v*) ethanol 2 times. Seeds were individually plated in sterile conditions on half-strength Murashige and Skoog (MS) medium [24] supplemented with 0.1% (*w/v*) sucrose, 0.05% (*w/v*) MES, pH 5.8, and 0.8% (*w/v*) plant agar. Plates were sealed with Micropore tape to allow gas exchange and avoid condensation. Plates were then vernalized and exposed to light for 14 h before being kept in darkness as previously described [20]. Plates were then transferred under either NNMF or GMF and exposed to $120 \mu\text{mol m}^{-2} \text{s}^{-1}$ light provided by a tunable LED lighting system source (PHYTOFY RL 150W, Osram, München, Germany) at 22°C ($\pm 1.5^\circ\text{C}$) with a 16/8 light/darkness photoperiod. For the entire experimental time, the temperature was set and maintained by air-conditioning. All experiments were performed under normal gravity and atmospheric pressure.

2.2. Near Null Magnetic Field (NNMF) Generation System and Plant Exposure

The GMF (or local geomagnetic field) values were typical of the northern hemisphere at $45^\circ 0' 59''$ N and $7^\circ 36' 58''$ E coordinates. Near-null magnetic field (NNMF) was generated as previously described [25]. Real-time monitoring of the MF in the plant exposure chamber was achieved with a three-axis magnetic field sensor (model Mag-03, Bartington Instruments, Oxford, UK) that was placed at the geometric center of the Helmholtz coils. The output data from the magnetometer were uploaded to a VEE Pro for Windows software release 7.51 (Agilent Technologies, Santa Clara, CA, USA; <https://www.keysight.com/it> accessed on 1 October 2022) to accurately adjust the current applied through each of the Helmholtz coil pairs in order to maintain the MF constant inside the plant growth chamber at NNMF intensity, as recently reported [20]. Plates containing *A. thaliana* seedlings seeded 134 h before were placed in the geometric center of the triaxial Helmholtz coils system and exposed either to NNMF for 10 min, 1 h, 2 h, 4 h, 24 h, 48 h, and 96 h. After the exposure period, shoots and roots were separately harvested and immediately frozen in liquid nitrogen.

2.3. RNA Extraction from Arabidopsis Shoots and Roots upon Time-Course Exposure to GMF and NNMF

For each time point, 100 mg of frozen *A. thaliana* roots or shoots exposed to either GMF or NNMF were ground in liquid nitrogen and total RNA was isolated and its quality and quantity checked as previously described [20]. Quantification of RNA was also confirmed spectrophotometrically by using a NanoDrop ND-1000 (Thermo Fisher Scientific, Waltham, MA, USA).

2.4. cDNA Synthesis and Gene Microarray Analyses (Including MIAME)

Five hundred nanograms of total RNA from each sample were separately reverse-transcribed into double-stranded cDNA, which was transcribed into antisense cRNA and labelled with either Cy3-CTP or Cy5-CTP fluorescent dyes for 2 h at 40 °C as reported before [21]. Cyanine-labeled cRNAs were purified using RNeasy Minikit (Qiagen, Hilden, Germany). Purity and dye incorporation were assessed as previously described [20]. Then, 825 ng of control Cy3-RNAs and 825 ng of treated Cy5-RNAs were pooled together and hybridized using the Gene Expression Hybridization Kit (Agilent Technologies) onto 4 × 44 K *A. thaliana* (v3) Oligo Microarray (Agilent Technologies). The microarray experiment followed a direct 2 × 2 factorial two-color design. This resulted in two-color arrays, satisfying Minimum Information About a Microarray Experiment (MIAME) requirements [26].

Microarrays were scanned as reported before [20] (Agilent Technologies).

GO enrichment information for the differently expressed probe sets was obtained from The *A. thaliana* information resource (<https://www.arabidopsis.org/index.jsp> accessed on 1 October 2022).

2.5. Validation of Microarray Data by Real-Time PCR

In order to validate microarray data, qPCR analyses were performed on a QuantStudio 3 Real-Time PCR System (Applied Biosystems, Foster City, CA, USA) using the same cDNA products obtained as previously described (Section 2.4). Amplification was carried out with the primers listed in Supplementary Table S1, while the reaction was performed using Maxima SYBR Green/ROX qPCR Master Mix Kit (Thermo Fisher Scientific, Waltham, MA, USA) in 25 µL of total volume. The thermocycling was performed using two-step cycling protocol: 50 °C for 2 min, 95 °C for 10 min, 95 °C for 15 s, and 60 °C for 60 s. The last two steps were repeated for 40 cycles. All primers were designed using Primer 3 software. Four different reference genes (cytoplasmic glyceraldehyde-3-phosphate dehydrogenase, (*GAPC2*, *At1g13440*), ubiquitin specific protease 6 (*UBP6*, *At1g51710*), actin1 (*ACT1*, *At2g37620*), and the elongation factor 1B alpha-subunit 2 (*eEF1Balpha2*, *At5g19510*)) were used to normalize the results of qPCR; the most stable gene was the ubiquitin specific protease 6 (*UBP6*). All amplification plots were analyzed with QuantStudio Design & Analysis software (Applied Biosystem, Foster City, CA, USA) to obtain Ct values. Relative RNA levels were calibrated and normalized with the level of the ubiquitin specific protease 6 (*UBP6*) mRNA.

2.6. Reactive Oxygen Species Quantification and Activity

Determination of the H₂O₂ content was carried out by using MAK311 Peroxide Assay Kit (Sigma-Aldrich, St. Louis, MI, USA). Roots and shoots of *A. thaliana* plants were sampled at different time points as described in paragraphs 2.1 and 2.2. Samples were grinded and extracted in 1:10 (*w/v*) mQ water. After centrifugation at 15,000 × *g* for 10 min, the supernatant was used for the assay. Four µL of each standard and sample were incubated for 30 min at RT with 20 µL of assay kit Detection Reagent. An optical density of 2 µL was measured at 585 nm with BioSpec-nano Spectrophotometer (Shimadzu, Kyoto, Japan).

2.7. Analysis of Antioxidant Molecules by HPLC-ESI-MS/MS

The same water-extracted samples used for ROS quantification (see Section 2.6) were immediately injected into an HPLC system (Agilent Technologies 1200, Santa Clara, CA, USA) coupled to a diode array detector (DAD) (Agilent Technologies 1200, Santa Clara, CA, USA). Additionally, analyses were performed by using a mass spectrometer (6330 Series Ion Trap Mass Spectrometer System, Agilent Technologies, Santa Clara, CA, USA) coupled to an electrospray ionization (ESI) module. The chromatographic separation was carried out using a constant flow rate (0.2 mL min⁻¹) through a reverse phase C18 Luna column (3.00 µm, 150 × 3.0 mm i.d., Phenomenex, CA, USA), maintained at 25 °C by an Agilent 1100 HPLC G1316A Column Compartment. The chromatographic separation was obtained by a binary solvent system consisting of MilliQ H₂O acidified with 0.1%

formic acid (*v/v*) (Solvent A) and Acetonitrile acidified with 0.1% formic acid (*v/v*) (Sigma-Aldrich, CA, USA) (Solvent B). The initial concentration of the solvents was set at 90% A and 10% B for 5 min, then the concentration of Solvent B was raised to 55% A in 25 min, and finally at 70% B in 25 min. The initial solvent concentration was restored at the end of each run and maintained for an additional 10 min before the next injection. Sample injection volume was set at 5 μL . For each injection, UV–VIS spectra were recorded at 220, 280, 360, and 520 nm, along with the whole UV/Vis spectrum between 200 and 800 nm. Tandem mass spectrometry analyses were performed operating in negative mode. The nitrogen flow rate was set at 15.0 mL min^{-1} and maintained at 350 $^{\circ}\text{C}$, whereas the capillary voltage was set at 1.5 kV. Analyses were performed in triplicate. The different compounds were identified by comparing the retention time (RT), UV–Vis, and MS/MS spectra with reference compounds. Finally, the quantification was performed using external calibration curves (range: 0.03–0.15 $\mu\text{g}/\text{mL}$). The results were expressed as $\mu\text{g g}^{-1}$ FW.

2.8. Statistical Analysis

The data obtained from qPCR, HPLC, and biochemical assays were treated by using Systat 10. Mean value was calculated along with the SD. Paired *t*-test and Bonferroni-adjusted probability were used to assess the difference between treatments and controls. Processing and statistical analysis of the microarray data were performed in R using Bioconductor package limma [27]. The raw microarray data were subjected to background subtraction and loess-normalized. Agilent control probes were filtered out. The linear models implemented in limma were used for finding DEGs. Comparisons were made for each of the treatment. Benjamini and Hochberg (BH) multiple testing correction was applied [28]. Heatmaps were obtained with Heatmapper (<http://www.heatmapper.ca/>; accessed on 1 September 2022) [29] by using Pearson clustering with single linkage method.

3. Results

3.1. Transcriptomic Analyses Reveal Differential Root/Shoot DEGs of Oxidative Stress-Related Activity in Plants Exposed to NNMF

A. thaliana seedlings vertically grown in Petri dishes and exposed to NNMF conditions from 10 min to 96 h were separately sampled by collecting roots and shoots. Controls plants were grown in the same experimental conditions (i.e., temperature, gravity, atmospheric pressure, and photosynthetic phlux density—PPD) but under GMF. Samples were assayed by microarray gene expression. Supplementary Dataset S1 collects all information on the gene expression fold change volcano plots for all evaluated time points. Gene microarray data were then filtered by considering all genes coding for enzymes involved in oxidative reactions. A total of 194 DEGs were selected. A consistent percentage of these DEGs explained a fold change value >2 at almost all time points (Supplementary Table S2). In the following text, the term “not regulated” is referred to genes that are DEGs with fold change values below the established threshold limits of >2 and <0.5 .

In general, the gene ontology (GO) analysis of the selected genes showed that the cellular component DEGs were mainly expressed in the extracellular region, followed by cytoplasm, cell wall, and chloroplast-related DEGs (Figure 1A), with a molecular function mainly identified in catalytic activity and binding (Figure 1B). The biological process was associated to DEGs responding to stress, and other cellular and metabolic processes (Figure 1C). The data matrix of Supplementary Table S2 was then subjected to heatmapping in order to identify specific root/shoot patterns of DEGs.

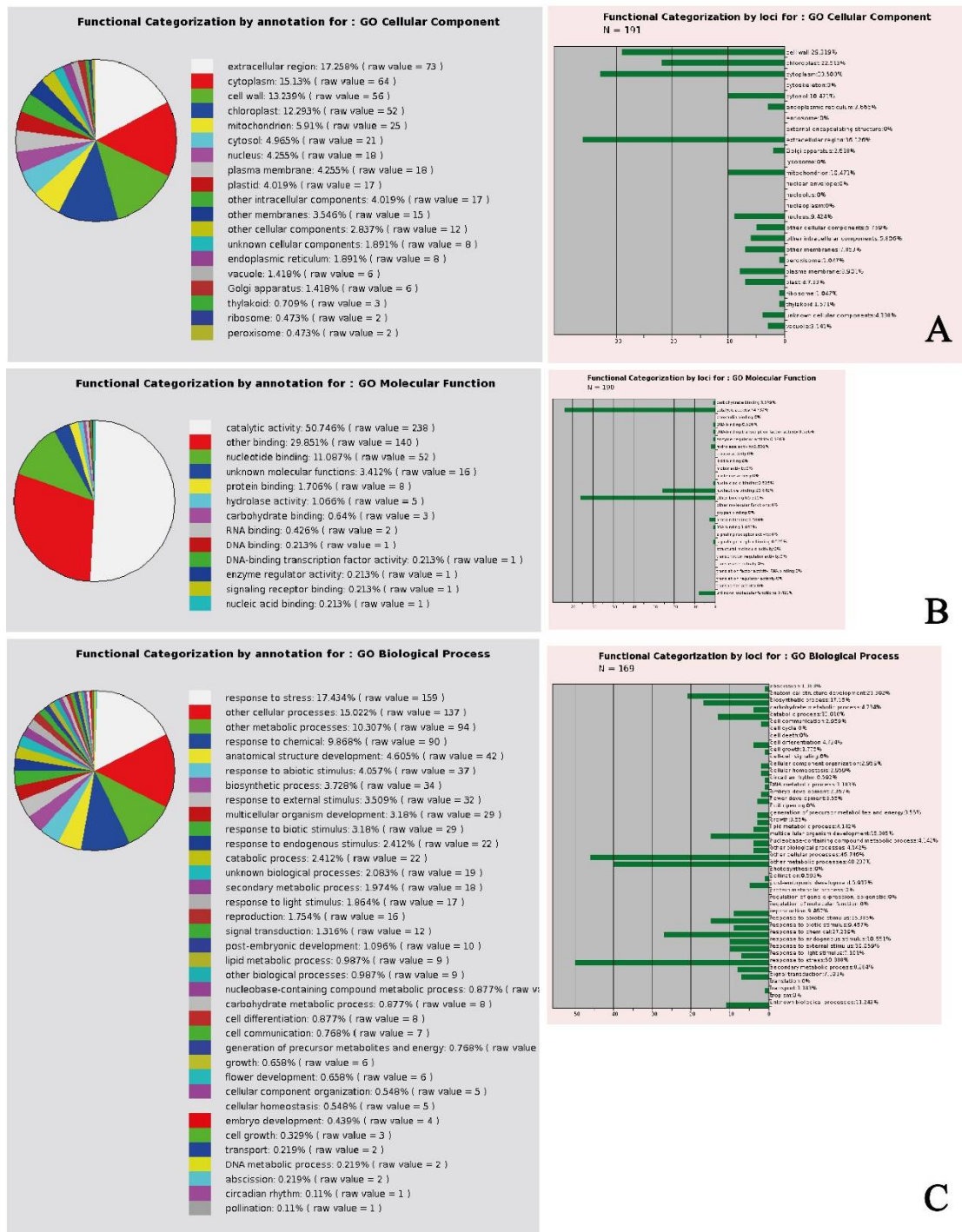


Figure 1. Gene ontology analysis of *Arabidopsis thaliana* genes selected for their involvement in oxidative stress. (A) Cellular component; (B) molecular function; (C) biological process. See text for further explanation.

Figure 2 shows the heatmap depicting the time-course DEGs of roots and shoots in plants grown under NMF with respect to GMF (this heatmap includes all DEGs). Based on the expression matrix, we selected five groups characterized by specific expression patterns (groups A–E), which were then organized in tables by selecting DEGs showing a fold change ≥ 2 or ≤ 0.5 in at least one time point (Tables 1–5). We identified three main timing of magnetic induction: (i) early (10 min to 2 h), (ii) intermediate (4 and 24 h), and (iii) late (48 and 96 h).

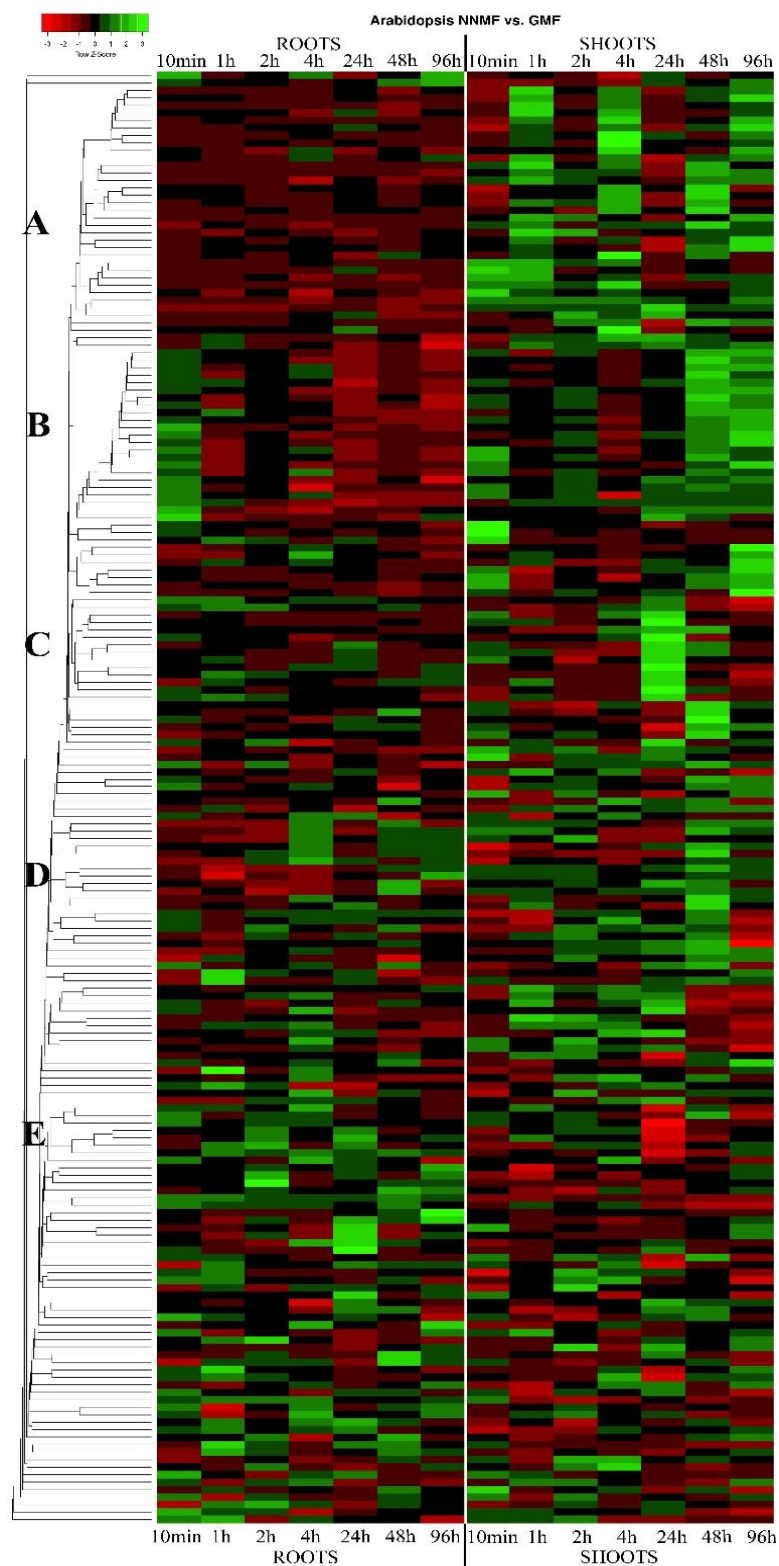


Figure 2. Heatmap of genes coding for enzymes involved in oxidation reactions from the time-course microarray gene expression of *A. thaliana* grown in a near-null magnetic field (NNMF) compared to geomagnetic field (GMF) grown plants. The heatmap was generated by using a single linkage clustering method and Pearson distance measuring method. Downregulated genes are marked in red-shaded colors, whereas upregulation is evidenced by different shades of green. Five groups of genes are evidenced (see text for more details).

Table 1. Group A. Genes not regulated or downregulated in roots and upregulated in shoots. Genes were selected based on a fold change ≥ 2 or ≤ 0.5 in at least one time point. Values are expressed as the mean and standard deviation (\pm), values with a fold change ≥ 2 or ≤ 0.5 are indicated as boldfaced numbers.

Gene Locus	Gene Code	ROOT							SHOOT						
		10 min	1 h	2 h	4 h	24 h	48 h	96 h	10 min	1 h	2 h	4 h	24 h	48 h	96 h
At4g37160	SKS15	0.75 \pm 0.16	0.77 \pm 0.08	0.93 \pm 0.08	0.82 \pm 0.11	0.92 \pm 0.21	0.76 \pm 0.18	0.67 \pm 0.03	0.72 \pm 0.11	1.16 \pm 0.54	0.58 \pm 0.4	2.00 \pm 0.65	1.03 \pm 0.22	0.99 \pm 0.38	1.10 \pm 0.61
At1g21860	SKS7	0.50 \pm 0.10	1.78 \pm 0.43	0.86 \pm 0.44	0.63 \pm 0.11	0.79 \pm 0.44	0.94 \pm 0.60	0.92 \pm 0.19	2.11 \pm 0.34	2.50 \pm 0.77	0.98 \pm 0.69	2.12 \pm 0.24	1.84 \pm 0.31	3.62 \pm 2.64	1.98 \pm 0.25
At4g25310	2OG and Fe(II)-dependent oxygenase	0.88 \pm 0.11	1.14 \pm 0.13	1.11 \pm 0.13	1.07 \pm 0.12	0.95 \pm 0.06	1.12 \pm 0.20	0.83 \pm 0.47	1.56 \pm 0.31	2.39 \pm 0.50	1.72 \pm 0.16	1.77 \pm 0.31	0.72 \pm 0.03	2.72 \pm 0.56	2.32 \pm 1.92
At1g55290	F6/H2	1.33 \pm 0.13	1.13 \pm 0.04	0.99 \pm 0.10	1.15 \pm 0.07	1.39 \pm 0.21	0.88 \pm 0.48	1.23 \pm 0.14	0.50 \pm 0.03	1.38 \pm 0.85	1.25 \pm 0.25	2.17 \pm 1.33	1.15 \pm 0.26	2.40 \pm 2.07	0.78 \pm 0.20
At5g51930	GMC	0.84 \pm 0.23	0.82 \pm 0.05	0.78 \pm 0.12	1.08 \pm 0.18	0.85 \pm 0.16	0.79 \pm 0.13	0.78 \pm 0.08	2.30 \pm 1.96	2.40 \pm 0.44	1.45 \pm 0.63	1.79 \pm 0.12	0.88 \pm 0.31	1.32 \pm 0.34	0.72 \pm 0.08
At1g19900	RUBY	1.00 \pm 0.10	0.98 \pm 0.11	0.93 \pm 0.1	0.96 \pm 0.12	1.51 \pm 0.84	0.67 \pm 0.43	0.75 \pm 0.06	1.05 \pm 0.41	0.62 \pm 0.22	1.02 \pm 0.26	2.49 \pm 1.32	0.55 \pm 0.37	0.92 \pm 0.08	0.65 \pm 0.21
At5g22410	RHS18	1.06 \pm 0.22	0.99 \pm 0.16	0.92 \pm 0.05	0.81 \pm 0.22	0.98 \pm 0.20	0.57 \pm 0.30	1.06 \pm 0.20	0.95 \pm 0.50	3.59 \pm 2.18	1.04 \pm 0.74	2.53 \pm 1.26	1.09 \pm 0.18	1.35 \pm 0.78	2.09 \pm 1.57
At5g48100	LAC15	1.28 \pm 0.18	0.90 \pm 0.15	1.34 \pm 0.15	0.64 \pm 0.16	1.37 \pm 0.21	1.14 \pm 0.23	0.96 \pm 0.11	2.25 \pm 1.78	1.45 \pm 0.26	1.36 \pm 1.05	1.50 \pm 0.35	1.23 \pm 0.78	1.00 \pm 0.22	1.65 \pm 0.53
At5g01050	LAC9	1.04 \pm 0.19	1.08 \pm 0.11	1.01 \pm 0.06	1.23 \pm 0.16	0.93 \pm 0.06	1.11 \pm 0.19	1.04 \pm 0.18	0.90 \pm 0.17	1.62 \pm 0.63	1.21 \pm 0.73	2.97 \pm 1.57	1.72 \pm 0.39	1.15 \pm 0.08	2.04 \pm 0.50
At1g48700	CP5	0.69 \pm 0.06	0.61 \pm 0.30	0.64 \pm 0.32	0.82 \pm 0.12	1.03 \pm 0.19	0.38 \pm 0.09	1.15 \pm 0.83	2.01 \pm 0.33	1.87 \pm 0.39	2.22 \pm 0.40	1.90 \pm 0.09	3.45 \pm 0.96	2.20 \pm 0.44	1.94 \pm 0.77
At1g05240	PR9	1.17 \pm 0.22	1.19 \pm 0.04	0.97 \pm 0.05	0.95 \pm 0.21	1.13 \pm 0.11	0.97 \pm 0.19	1.01 \pm 0.25	0.61 \pm 0.08	2.02 \pm 0.87	1.06 \pm 0.67	1.86 \pm 1.34	0.92 \pm 0.22	1.44 \pm 0.18	2.32 \pm 0.75
At1g05250	PRX2	0.95 \pm 0.17	1.07 \pm 0.03	0.89 \pm 0.05	0.86 \pm 0.21	1.01 \pm 0.13	0.83 \pm 0.16	0.98 \pm 0.28	0.58 \pm 0.07	1.79 \pm 1.32	0.99 \pm 0.75	2.83 \pm 1.93	0.67 \pm 0.17	1.23 \pm 0.19	2.18 \pm 0.56
At1g30870	PER7	1.02 \pm 0.19	1.02 \pm 0.07	0.93 \pm 0.05	0.91 \pm 0.19	1.27 \pm 0.20	0.95 \pm 0.24	1.02 \pm 0.16	0.54 \pm 0.10	1.10 \pm 0.69	1.03 \pm 0.73	2.07 \pm 1.07	0.67 \pm 0.08	2.26 \pm 2.10	1.20 \pm 0.14
At1g34510	PER8	1.16 \pm 0.18	0.90 \pm 0.08	1.04 \pm 0.23	1.13 \pm 0.08	1.53 \pm 1.17	0.60 \pm 0.49	1.23 \pm 0.49	0.67 \pm 0.12	3.28 \pm 2.67	1.27 \pm 0.58	2.42 \pm 2.35	0.57 \pm 0.29	1.93 \pm 0.34	2.67 \pm 0.79
At1g49570	PER10	0.72 \pm 0.14	0.82 \pm 0.13	1.03 \pm 0.14	0.73 \pm 0.22	0.99 \pm 0.32	0.92 \pm 0.21	0.57 \pm 0.48	0.72 \pm 0.13	0.86 \pm 0.45	0.37 \pm 0.27	1.69 \pm 0.78	0.96 \pm 0.06	2.14 \pm 1.31	0.90 \pm 0.55
At2g43480	PER26	0.85 \pm 0.18	0.91 \pm 0.09	0.92 \pm 0.02	0.82 \pm 0.04	0.88 \pm 0.14	0.93 \pm 0.06	0.82 \pm 0.05	1.06 \pm 0.30	2.05 \pm 0.04	1.75 \pm 0.34	1.10 \pm 0.26	0.55 \pm 0.14	1.05 \pm 0.18	2.09 \pm 0.23
At4g26010	PRX44	1.18 \pm 0.22	1.10 \pm 0.15	0.99 \pm 0.03	0.99 \pm 0.27	1.01 \pm 0.16	0.98 \pm 0.27	1.11 \pm 0.10	1.59 \pm 0.23	2.66 \pm 1.22	1.39 \pm 0.55	2.06 \pm 1.35	0.77 \pm 0.19	2.33 \pm 2.19	1.31 \pm 0.33
At5g24070	PER61	1.01 \pm 0.1	1.14 \pm 0.19	1.12 \pm 0.11	1.13 \pm 0.09	1.70 \pm 0.78	0.84 \pm 0.32	0.79 \pm 0.11	3.39 \pm 4.57	3.23 \pm 2.41	0.85 \pm 0.56	1.52 \pm 0.06	0.90 \pm 0.42	1.46 \pm 0.54	1.12 \pm 1.01
At5g67400	PRX73	1.03 \pm 0.17	1.15 \pm 0.20	1.01 \pm 0.11	1.01 \pm 0.19	1.21 \pm 0.18	1.03 \pm 0.28	1.23 \pm 0.21	0.62 \pm 0.03	2.08 \pm 0.68	1.58 \pm 0.83	2.21 \pm 1.38	0.72 \pm 0.07	2.25 \pm 1.88	1.11 \pm 0.20
At1g67270	Monoamine-oxidase A repressor R1 protein	0.96 \pm 0.13	0.99 \pm 0.08	0.93 \pm 0.16	0.88 \pm 0.31	0.92 \pm 0.17	0.71 \pm 0.09	0.70 \pm 0.38	2.14 \pm 0.33	2.21 \pm 0.12	2.32 \pm 0.41	2.11 \pm 0.25	1.97 \pm 0.54	1.69 \pm 0.91	2.34 \pm 0.78

Table 2. Group B. Genes that are upregulated in shoots mostly at all times and upregulated in roots mainly at earlier times. Genes were selected based on a fold change ≥ 2 or ≤ 0.5 in at least one time point. Values are expressed as the mean and standard deviation (\pm), values with a fold change ≥ 2 or ≤ 0.5 are indicated as boldfaced numbers.

Gene Locus	Gene Code	ROOT							SHOOT						
		10 min	1 h	2 h	4 h	24 h	48 h	96 h	10 min	1 h	2 h	4 h	24 h	48 h	96 h
At3g59845	Zinc-binding dehydrogenase family protein	2.35 \pm 0.30	1.88 \pm 0.15	2.13 \pm 0.19	2.49 \pm 0.52	1.89 \pm 0.21	1.99 \pm 0.30	1.91 \pm 0.11	2.38 \pm 0.58	2.10 \pm 0.11	2.28 \pm 0.43	2.07 \pm 0.27	2.21 \pm 0.60	2.47 \pm 0.36	2.27 \pm 0.34
At4g28090	SKS10	2.50 \pm 0.36	1.88 \pm 0.14	2.14 \pm 0.20	2.28 \pm 0.31	1.95 \pm 0.20	2.02 \pm 0.33	1.92 \pm 0.11	2.61 \pm 0.32	2.14 \pm 0.13	2.21 \pm 0.49	1.94 \pm 0.08	2.10 \pm 0.52	2.40 \pm 0.35	2.37 \pm 0.36
At1g55570	SKS12	2.70 \pm 0.49	1.99 \pm 0.11	2.24 \pm 0.21	1.92 \pm 0.23	2.13 \pm 0.20	2.13 \pm 0.35	2.04 \pm 0.11	2.05 \pm 0.92	2.20 \pm 0.18	2.45 \pm 0.61	1.87 \pm 0.17	2.51 \pm 0.47	2.76 \pm 1.93	3.35 \pm 1.75
At1g75790	SKS18	3.03 \pm 1.00	1.91 \pm 0.12	1.85 \pm 0.29	1.61 \pm 0.49	2.03 \pm 0.22	1.89 \pm 0.09	2.28 \pm 0.45	2.26 \pm 0.38	2.27 \pm 0.22	2.25 \pm 0.51	2.09 \pm 0.27	2.00 \pm 0.86	2.89 \pm 0.45	2.73 \pm 0.68
At1g21850	SKS8	2.34 \pm 0.29	1.87 \pm 0.15	2.12 \pm 0.19	2.09 \pm 0.42	1.89 \pm 0.20	1.98 \pm 0.30	1.72 \pm 0.27	2.35 \pm 0.29	2.13 \pm 0.13	2.27 \pm 0.43	2.07 \pm 0.27	2.21 \pm 0.60	2.62 \pm 0.44	2.53 \pm 0.43
At1g32710	Cytochrome c oxidase	2.51 \pm 0.35	1.98 \pm 0.12	2.28 \pm 0.27	2.03 \pm 0.28	2.02 \pm 0.20	2.13 \pm 0.42	2.03 \pm 0.11	2.31 \pm 0.33	2.19 \pm 0.14	2.47 \pm 0.33	2.13 \pm 0.31	2.26 \pm 0.53	2.60 \pm 0.58	2.94 \pm 0.35

Table 2. Cont.

Gene Locus	Gene Code	ROOT							SHOOT						
		10 min	1 h	2 h	4 h	24 h	48 h	96 h	10 min	1 h	2 h	4 h	24 h	48 h	96 h
<i>At1g28030</i>	<i>2OG-Fe(II)-oxygenase</i>	2.33 ± 0.38	1.89 ± 0.13	2.16 ± 0.20	1.81 ± 0.77	1.93 ± 0.24	2.01 ± 0.31	1.90 ± 0.13	2.32 ± 0.37	2.10 ± 0.03	2.06 ± 0.44	2.10 ± 0.29	1.99 ± 0.51	2.22 ± 0.23	2.60 ± 0.53
<i>At1g52790</i>	<i>2OG-Fe(II)-oxygenase</i>	2.53 ± 0.32	2.00 ± 0.13	2.22 ± 0.30	1.83 ± 0.29	1.82 ± 0.32	2.21 ± 0.35	1.00 ± 0.50	2.14 ± 0.14	2.25 ± 0.18	2.29 ± 0.31	2.12 ± 0.32	2.46 ± 0.52	2.36 ± 0.17	2.46 ± 0.45
<i>At2g44800</i>	<i>2OG-Fe(II)-oxygenase</i>	2.22 ± 0.41	2.15 ± 0.57	2.14 ± 0.19	2.09 ± 0.42	1.99 ± 0.24	1.93 ± 0.39	1.86 ± 0.11	2.20 ± 0.38	2.15 ± 0.13	2.28 ± 0.42	1.94 ± 0.43	2.19 ± 0.60	2.45 ± 0.32	2.57 ± 0.46
<i>At3g28490</i>	<i>2OG-Fe(II)-oxygenase</i>	2.45 ± 0.33	2.18 ± 0.46	2.21 ± 0.19	2.37 ± 0.39	1.94 ± 0.18	2.07 ± 0.36	1.99 ± 0.10	2.20 ± 0.30	2.15 ± 0.12	2.26 ± 0.34	2.07 ± 0.29	2.20 ± 0.54	2.73 ± 0.53	2.62 ± 0.57
<i>At1g60980</i>	<i>GA2OX4</i>	2.36 ± 0.29	2.11 ± 0.49	2.13 ± 0.20	1.94 ± 0.29	1.90 ± 0.19	2.01 ± 0.38	1.88 ± 0.13	2.21 ± 0.39	2.13 ± 0.13	2.26 ± 0.42	2.08 ± 0.27	2.21 ± 0.60	2.86 ± 0.44	2.54 ± 0.44
<i>At2g34555</i>	<i>GA2OX3</i>	2.38 ± 0.42	2.18 ± 1.05	1.50 ± 0.25	1.05 ± 0.46	0.68 ± 0.26	0.99 ± 0.48	0.84 ± 0.60	1.41 ± 0.18	2.12 ± 0.12	2.17 ± 0.40	2.00 ± 0.29	2.17 ± 0.57	2.29 ± 0.30	2.11 ± 0.21
<i>At1g11770</i>	<i>OGOX3</i>	2.38 ± 0.31	1.88 ± 0.13	2.14 ± 0.20	2.20 ± 0.41	1.90 ± 0.18	2.02 ± 0.33	1.91 ± 0.13	2.71 ± 0.69	2.13 ± 0.13	2.44 ± 0.45	1.98 ± 0.14	2.19 ± 0.60	2.64 ± 0.50	2.36 ± 0.39
<i>At4g20800</i>	<i>ATBBE17</i>	2.36 ± 0.30	2.11 ± 0.47	2.15 ± 0.21	2.09 ± 0.40	1.87 ± 0.20	2.01 ± 0.31	1.92 ± 0.16	2.31 ± 0.25	1.96 ± 0.39	2.27 ± 0.39	2.05 ± 0.25	2.17 ± 0.58	2.67 ± 0.50	2.59 ± 0.51
<i>At2g38960</i>	<i>AERO2</i>	2.23 ± 0.08	1.86 ± 0.13	2.10 ± 0.17	2.07 ± 0.42	1.85 ± 0.28	2.18 ± 0.49	1.71 ± 0.13	2.33 ± 0.28	2.17 ± 0.12	2.36 ± 0.43	2.04 ± 0.27	2.19 ± 0.51	2.81 ± 0.44	2.55 ± 0.57
<i>At1g32300</i>	<i>GulLO1</i>	3.05 ± 0.84	2.15 ± 0.45	2.15 ± 0.19	2.34 ± 0.37	1.81 ± 0.36	2.04 ± 0.34	1.96 ± 0.09	2.20 ± 0.32	2.20 ± 0.13	2.25 ± 0.35	2.06 ± 0.28	2.20 ± 0.56	2.70 ± 0.52	3.01 ± 1.26
<i>At5g45180</i>	<i>Monoxygenase</i>	2.37 ± 0.31	2.19 ± 0.51	2.13 ± 0.15	1.66 ± 0.85	1.73 ± 0.04	1.91 ± 0.39	1.69 ± 0.12	2.19 ± 0.38	2.13 ± 0.13	2.25 ± 0.41	2.05 ± 0.28	2.23 ± 0.56	2.63 ± 0.50	2.74 ± 0.30
<i>At1g14430</i>	<i>GOXL5</i>	2.36 ± 0.29	2.39 ± 0.81	2.19 ± 0.22	2.24 ± 0.30	1.87 ± 0.20	2.04 ± 0.37	1.90 ± 0.14	2.32 ± 0.26	2.14 ± 0.11	2.23 ± 0.34	2.05 ± 0.25	2.34 ± 0.59	2.66 ± 0.50	2.58 ± 0.50
<i>At5g09360</i>	<i>LAC14</i>	3.66 ± 0.84	1.22 ± 0.08	1.71 ± 0.36	1.66 ± 0.41	1.77 ± 0.33	1.33 ± 0.57	2.41 ± 0.41	2.22 ± 0.28	2.07 ± 0.18	1.95 ± 0.01	1.94 ± 0.06	3.35 ± 0.88	2.41 ± 0.21	1.56 ± 0.77
<i>At3g45810</i>	<i>RBOHJ</i>	2.00 ± 0.37	1.87 ± 0.15	2.15 ± 0.21	2.25 ± 0.31	1.83 ± 0.20	1.97 ± 0.31	1.93 ± 0.13	2.15 ± 0.33	2.12 ± 0.13	2.17 ± 0.29	2.02 ± 0.27	2.14 ± 0.55	2.80 ± 0.51	2.36 ± 0.47
<i>At1g65990</i>	<i>PRXIIA</i>	2.21 ± 0.04	2.40 ± 0.81	2.20 ± 0.21	2.10 ± 0.53	1.85 ± 0.20	1.81 ± 0.16	1.83 ± 0.12	2.02 ± 0.21	2.13 ± 0.13	2.25 ± 0.35	2.03 ± 0.28	2.17 ± 0.58	2.62 ± 0.50	2.64 ± 0.10
<i>At1g24110</i>	<i>PER6</i>	2.46 ± 0.39	2.14 ± 0.57	2.19 ± 0.21	2.26 ± 0.34	1.76 ± 0.42	1.86 ± 0.37	1.84 ± 0.26	2.41 ± 0.36	2.04 ± 0.27	2.20 ± 0.48	1.50 ± 0.28	2.29 ± 0.78	2.23 ± 0.46	2.36 ± 0.38
<i>At3g42570</i>	<i>Peroxidase</i>	2.35 ± 0.31	1.93 ± 0.17	2.09 ± 0.22	1.40 ± 0.75	1.89 ± 0.22	1.99 ± 0.30	1.87 ± 0.05	2.36 ± 0.28	2.10 ± 0.11	2.28 ± 0.42	2.07 ± 0.27	2.22 ± 0.59	2.48 ± 0.37	2.21 ± 0.42

Table 3. Group C. Genes characterized by a strong upregulation in shoots at 24 h. Genes were selected based on a fold change ≥ 2 or ≤ 0.5 in at least one time point. Values are expressed as the mean and standard deviation (\pm), values with a fold change ≥ 2 or ≤ 0.5 are indicated as boldfaced numbers.

Gene Locus	Gene Code	ROOT							SHOOT						
		10 min	1 h	2 h	4 h	24 h	48 h	96 h	10 min	1 h	2 h	4 h	24 h	48 h	96 h
<i>At1g26390</i>	<i>ATBBE4</i>	2.06 ± 0.56	1.80 ± 1.49	1.21 ± 0.99	0.58 ± 0.27	0.77 ± 0.09	1.49 ± 0.69	0.83 ± 0.45	3.22 ± 1.39	2.40 ± 0.55	1.22 ± 0.56	1.84 ± 1.19	6.89 ± 4.90	1.26 ± 0.71	0.52 ± 0.64
<i>At1g26410</i>	<i>ATBBE6</i>	0.29 ± 0.10	1.46 ± 1.02	0.87 ± 0.52	0.81 ± 0.18	0.60 ± 0.05	1.44 ± 0.18	1.22 ± 1.22	0.59 ± 0.12	1.72 ± 0.15	0.73 ± 0.50	0.60 ± 0.31	2.85 ± 3.47	0.55 ± 0.13	0.32 ± 0.26
<i>At4g21830</i>	<i>MSRB7</i>	0.97 ± 0.15	1.03 ± 0.17	0.92 ± 0.16	0.88 ± 0.07	0.90 ± 0.24	0.87 ± 0.43	0.84 ± 0.14	1.88 ± 1.83	0.67 ± 0.49	0.81 ± 0.07	1.75 ± 0.35	2.36 ± 1.14	1.27 ± 1.08	0.85 ± 0.21
<i>At5g05340</i>	<i>PRX52</i>	0.87 ± 0.09	1.11 ± 0.24	1.21 ± 0.30	0.88 ± 0.26	1.84 ± 1.08	0.91 ± 0.18	1.08 ± 0.25	1.40 ± 0.18	0.95 ± 0.05	0.92 ± 0.18	0.75 ± 0.11	2.36 ± 2.79	1.70 ± 0.28	0.91 ± 0.49

Table 4. Group D. Genes characterized by a strong upregulation in shoots at 48 h. Genes were selected based on a fold change ≥ 2 or ≤ 0.5 in at least one time point. Values are expressed as the mean and standard deviation (\pm), values with a fold change ≥ 2 or ≤ 0.5 are indicated as boldfaced numbers.

Gene Locus	Gene Code	ROOT							SHOOT						
		10 min	1 h	2 h	4 h	24 h	48 h	96 h	10 min	1 h	2 h	4 h	24 h	48 h	96 h
<i>At2g38240</i>	<i>AO4</i>	0.90 \pm 0.12	0.99 \pm 0.11	0.79 \pm 0.28	1.00 \pm 0.09	1.83 \pm 0.79	0.87 \pm 0.17	1.17 \pm 0.20	0.61 \pm 0.12	1.91 \pm 0.89	0.64 \pm 0.19	0.98 \pm 0.70	0.38 \pm 0.25	2.56 \pm 2.12	1.08 \pm 0.05
<i>At5g56470</i>	<i>GULLO7</i>	2.00 \pm 0.54	1.28 \pm 0.69	2.40 \pm 1.04	1.34 \pm 0.42	1.96 \pm 0.18	1.46 \pm 0.92	1.03 \pm 0.24	1.48 \pm 0.34	1.63 \pm 0.57	2.21 \pm 0.46	2.06 \pm 0.47	2.12 \pm 0.68	2.71 \pm 0.59	2.12 \pm 0.55
<i>At5g23990</i>	<i>FRO5</i>	1.44 \pm 0.31	0.60 \pm 0.46	0.85 \pm 0.03	0.81 \pm 0.27	1.44 \pm 0.58	2.03 \pm 0.35	1.98 \pm 0.09	2.17 \pm 0.31	2.13 \pm 0.11	2.22 \pm 0.38	1.91 \pm 0.03	2.10 \pm 0.63	2.70 \pm 0.53	1.95 \pm 0.24
<i>At3g56350</i>	<i>MSD2</i>	0.60 \pm 0.07	0.60 \pm 0.32	0.71 \pm 0.14	2.13 \pm 0.51	1.41 \pm 0.03	0.63 \pm 0.22	1.23 \pm 0.16	0.56 \pm 0.12	1.64 \pm 0.14	0.93 \pm 0.27	0.91 \pm 0.16	1.10 \pm 0.85	2.89 \pm 2.88	1.78 \pm 0.16
<i>At3g50990</i>	<i>PER36</i>	1.09 \pm 0.08	1.90 \pm 0.15	2.29 \pm 0.36	2.53 \pm 0.28	2.23 \pm 0.50	2.25 \pm 1.21	1.36 \pm 0.36	3.76 \pm 1.48	2.21 \pm 0.20	2.77 \pm 0.30	2.08 \pm 0.27	0.98 \pm 0.12	5.27 \pm 3.73	2.11 \pm 0.10

Table 5. Group E. Genes downregulated in shoots at 24 h. Genes selected based on a fold change ≥ 2 or ≤ 0.5 in at least one time point. Values are expressed as the mean and standard deviation (\pm), values with a fold change ≥ 2 or ≤ 0.5 are indicated as boldfaced numbers.

Gene Locus	Gene Code	ROOT							SHOOT						
		10 min	1 h	2 h	4 h	24 h	48 h	96 h	10 min	1 h	2 h	4 h	24 h	48 h	96 h
<i>At1g18490</i>	<i>PCO3</i>	0.89 \pm 0.24	1.38 \pm 0.33	1.62 \pm 0.35	0.92 \pm 0.18	1.32 \pm 0.24	0.78 \pm 0.07	1.01 \pm 0.12	0.74 \pm 0.12	0.75 \pm 0.17	1.15 \pm 0.58	1.27 \pm 0.57	0.49 \pm 0.10	1.01 \pm 0.48	1.18 \pm 0.25

Table 1 lists the DEGs of group A (Figure 2) showing a fold change ≥ 2 or ≤ 0.5 in at least one time point that are not regulated or downregulated in roots and upregulated in shoots. Most of the DEGs in this group have a subcellular prediction in the extracellular space and belong to the peroxidase family proteins, followed by laccases and dioxygenases (Supplementary Table S2). In particular, several shoot peroxidases (*At1g34510*, *At2g43480*, *At5g24070*, *At1g05240*, *At4g26010*, *At5g67400*) were upregulated at early (10 min and 1 h) times, whereas the peroxidases *At1g30870*, *At1g49570*, and *At1g05250* were upregulated in intermediate (4 h) and late (48–96 h) times. In shoots, *At1g48700*, a 2-oxoglutarate (2OG) and Fe(II)-dependent oxygenase, was upregulated at almost all times and downregulated in roots at 48 h, whereas three other 2OG-Fe(II) oxygenases were upregulated at early (*At5g51930*), middle and late times (*At1g55290*) and at early and late times (*At4g25310*). In shoots, a gene that encodes a protein that is similar to laccase-like polyphenol oxidases (*At5g48100*) was upregulated at very early times, whereas a putative laccase (*At5g01050*) was upregulated at intermediate and late times. A gene coding for a multicopper oxidase type I family protein (*At1g21860*) was downregulated at early times in roots and upregulated at almost all times in shoots, whereas a gene with a similar function (*At1g21860*) was only upregulated in shoots at intermediate times (Table 1).

Table 2 lists the DEGs of group B (Figure 2) that are upregulated in shoots mostly at all times and upregulated in roots mainly at earlier and intermediate times. Even in this group, some DEGs had an extracellular prediction but many were cytosolic. The gene function was dominated by copper ion binding oxidoreductases, dioxygenases, FAD-binding oxidases, and a few peroxidases (Supplementary Table S2). Four DEGs coding for 2OG-Fe(II) oxygenases (*At1g28030*, *At1g52790*, *At2g44800*, and *At3g28490*), two for gibberellin dioxygenases (*At1g60980* and *At2g34555*), and four DEGs coding for oxidoreductases with copper ion binding activity (*At4g28090*, *At1g55570*, *At1g75790*, and *At1g21850*) were upregulated in shoots at all times and upregulated in roots at early/intermediate times. Five DEGs coding for oxidoreductases with a FAD-binding domain (*At1g11770*, *At4g20800*, *At2g38960*, *At1g32300*, and *At5g45180*) were always upregulated in shoots, whereas in roots upregulation was absent at late times and the same pattern was observed for three peroxidases (*At1g65990*, *At1g24110*, and *At3g42570.1*) (Supplementary Table S2).

DEGs of group C (Figure 2) with a fold change ≥ 2 or ≤ 0.5 are listed in Table 3. Group C contains DEGs that are highly upregulated in shoots at 24 h (Figure 1). Two cytoplasmic DEGs encoding for oxidoreductases with a FAD-binding domain were both upregulated in shoots at 24 h, but one of them (*At1g26410.1*) was downregulated in roots at earlier time stages, whereas the other (*At1g26390.1*) was upregulated at earlier times both in roots and shoots. A gene coding for a peroxidase (*At5g05340.1*) with extracellular localization and a chloroplastic methionine sulfoxide reductase (*At4g21830.1*), which respond to singlet oxygen, were only upregulated in shoots at 24 h (Supplementary Table S2).

Group D contains DEGs that are highly upregulated in shoots at 48 h (Figure 2). DEGs of this group with a fold change ≥ 2 or ≤ 0.5 are listed in Table 4. A gene localized in the cytoplasm coding for a jasmonate-induced dioxygenase (*At2g38240.1*) was only upregulated in shoots at 48 h whereas another cytosolic gene coding for a galactose-oxidase (*At3g57620.1*) showed a high upregulation at 48 h also in roots. A gene coding for a plasma membrane-located ferric-chelate reductase (*At5g23990.1*) was upregulated in shoots at almost all times and upregulated in roots at 48 h, whereas a gene coding for an extracellular peroxidase (*At3g50990.1*) was highly upregulated in shoots at 48 h and was also upregulated in roots at intermediate and late times (Supplementary Table S2).

The last group, E, is made by DEGs that are downregulated in shoots at 24 h (Figure 2). The only gene with a fold change ≥ 2 or ≤ 0.5 (Table 5) is coding for a putative 2-aminoethanethiol dioxygenase (*At1g18490.1*) (Supplementary Table S2).

3.2. Validation by Real-Time PCR Confirms Gene Microarray Expression Data

Three genes were selected in order to validate the general gene expression of microarray results and were tested at 96 h. The pattern of fold change of *At2g18140*, *At1g32300*, and

At3g56350 (Table 6) was in line with the gene expression reported in the gene microarray experiments (see Supplementary Table S2).

Table 6. Validation of gene microarrays by qPCR. Fold change of NNMF expression vs. GMF expression of *Arabidopsis thaliana* exposed for 96 h. Values are expressed as means of at least three biological replicates (\pm standard deviation).

Gene Locus	FC Roots	FC Shoots
<i>At2g18140</i>	0.10 \pm 0.02	5.95 \pm 0.12
<i>At1g32300</i>	2.60 \pm 0.43	3.08 \pm 0.25
<i>At3g56350</i>	0.70 \pm 0.10	2.84 \pm 0.34

3.3. GMF Induces a Significant ROS Production

In order to evaluate the ROS production in NNMF conditions, we measured the H₂O₂ content during the middle and late stages of plant growth (24 h, 48 h, and 96 h). For technical reasons, measurements at early times were not possible due to the tiny amount of material. Analyses were performed on both roots and shoots of plants grown in GMF and NNMF.

In general, the content of H₂O₂ was reduced 5-fold at 24 h, 2-fold at 48 h, and 0.2-fold at 24 h in plants grown under NNMF in comparison to GMF condition, independently of the analyzed plant tissue (Table 7).

Table 7. Time-course analysis of H₂O₂ production in *Arabidopsis thaliana* under GMF and NNMF. Values are expressed as mmol H₂O₂ and fold change (NNMF/GMF). Within the same column, the letters indicate statistical difference ($p < 0.05$) among shoots (lowercase letters) or roots (uppercase letters), as measured by one-way ANOVA followed by Tukey's test. p values refer to the statistical difference in H₂O₂ content of samples grown under GMF and NNMF with the same sampling timing. For further statistical information see Supplementary Table S3.

Organ	Timing	GMF mmol H ₂ O ₂	NNMF mmol H ₂ O ₂	NNMF/GMF	p Value
Shoots	24 h	0.092 \pm 0.006 ^a	0.025 \pm 0.003 ^a	0.276 \pm 0.067	<0.001
	48 h	0.047 \pm 0.005 ^b	0.025 \pm 0.006 ^a	0.528 \pm 0.002	0.001
	96 h	0.016 \pm 0.001 ^c	0.013 \pm 0.003 ^b	0.805 \pm 0.006	0.006
Roots	24 h	0.051 \pm 0.006 ^A	0.014 \pm 0.001 ^A	0.274 \pm 0.034	<0.001
	48 h	0.040 \pm 0.007 ^A	0.025 \pm 0.001 ^B	0.625 \pm 0.031	0.011
	96 h	0.050 \pm 0.005 ^A	0.041 \pm 0.003 ^C	0.834 \pm 0.080	0.013

Under GMF, the shoot H₂O₂ content decreased with time, whereas under NNMF, the H₂O₂ concentration was practically unaffected at 24 and 48 h and significantly decreased only at 96 h (Table 7). By calculating the NNMF/GMF ratio, a general increasing trend was observed for both shoots and roots. In shoots, NNMF always showed highly significantly ($p < 0.01$) lower H₂O₂ production with respect to GMF (Table 7).

Under GMF, root H₂O₂ production was almost constant with time, whereas a significant ($p < 0.05$) increase in H₂O₂ was observed with time in roots exposed to NNMF (Table 7). However, as for shoots, the NNMF/GMF ratio indicated a general reduction of root H₂O₂ in NNMF exposed plants (Table 7).

Because the observed trend could be related to different DEGs involved in H₂O₂ metabolism, DEGs involved in H₂O₂ metabolic processes were extracted from Supplementary Table S2 (see Supplementary Table S4). These genes were then used to generate a heatmap calculated using a Pearson distance and average linkage method (Figure 3).

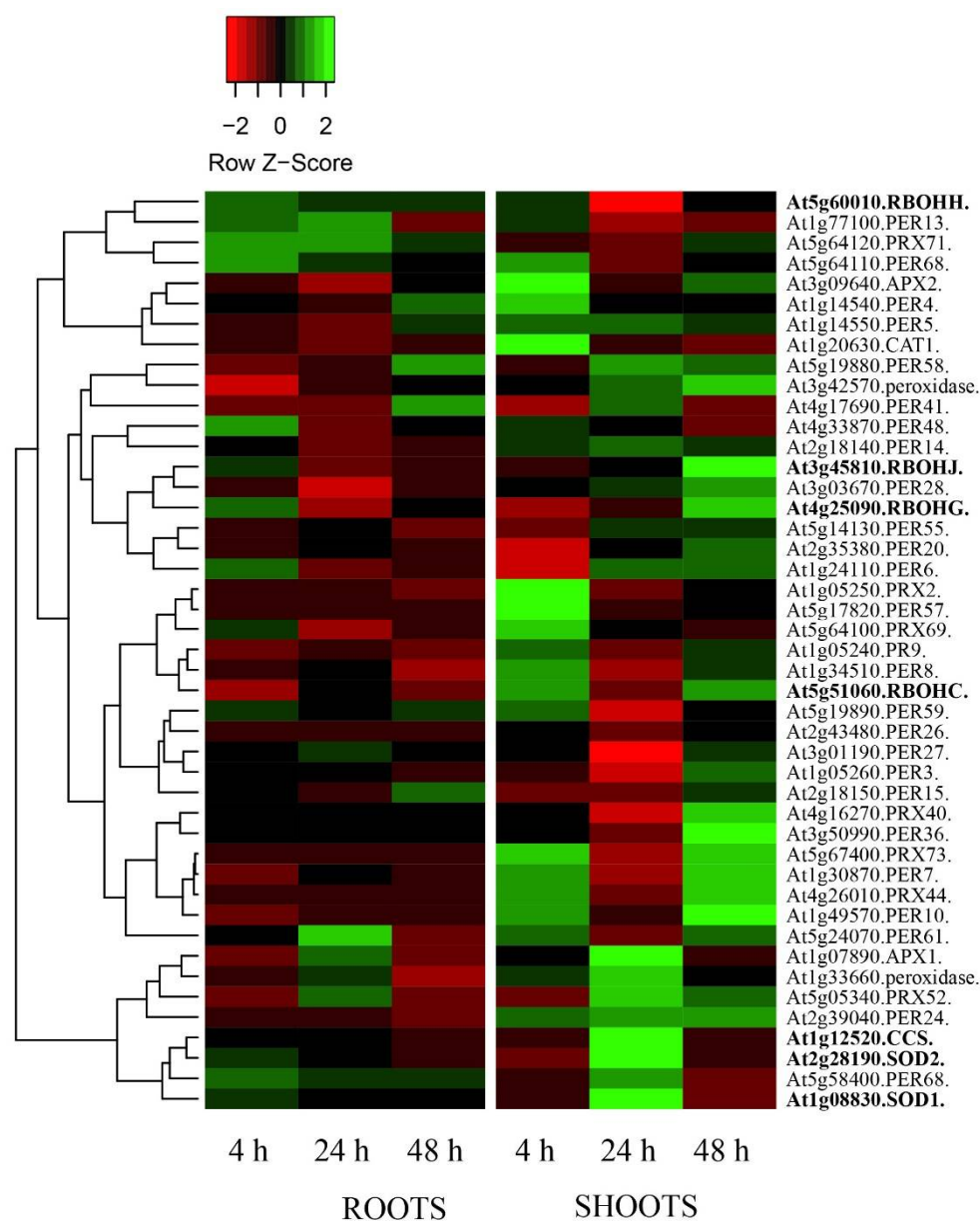


Figure 3. Gene expression fold change heatmap calculated with a Pearson distance and average linkage method from genes coding for ROS-scavenging enzymes selected from Supplementary Table S2 (see Supplementary Table S4). The heatmap was generated by using a single linkage clustering method and Pearson distance measuring method. Gene coding for ROS-producing enzymes are evidenced in boldface. Downregulated genes are marked in red-shaded colors, whereas upregulation is evidenced by different shades of green.

DEGs (NNMF/GMF fold change ratio) were considered by analyzing data from 4 h to 48 h in order to evaluate the possible regulation before the first (24 h) and last (96 h) time considered for ROS scavenging/production (Table 7). In general, the heatmap confirms the DEGs regulation of roots and shoots ROS-scavenging enzymes. In particular, roots showed a marked downregulation of most of DEGs responsible for the transcription of ROS-scavenging enzymes. The only exception was for *RBOHH* and *RBOHG* at 4 h and some peroxidases at 4 h (*PRX71*, *At1g77100*, *At5g64110*, *At4g33870*, *At5g58400*), 24 h (*PRX71*, *At1g77100*, *At5g24070*) and 48 h (*At1g77100*, *At5g19880*, *At4g17690*, *At2g18150*), which were upregulated (Figure 3). These data are in agreement with the general time-course increasing H_2O_2 levels in roots exposed to NNMF (Table 7). On the other hand, shoot upregulation of most of ROS-scavenging DEGs was evident (Figure 3), with stronger upregulation present

at 4 h for *CAT1* (*At1g20630*), *APX2* (*At3g09640*), *PRX2* (*At1g05250*), and *PER57* (*At5g17820*); at 24 h for *APX1* (*At1g07890*), *CCS* (*At1g12520*), *SOD1* (*At1g08830*), and *SOD2* (*At2g28190*); and at 48 h for *RBOHJ* (*At3g45810*), *RBOHG* (*At4g25090*), and *PER36* (*At3g50990*). Again, DEGs data obtained by microarray were in agreement with the decreasing shoot H₂O₂ production with time in NNMF exposed plants (Table 7).

3.4. Reduction of GMF to NNMF Modulates the Production of Antioxidant Polyphenols

HPLC-DAD-MS/MS analyses were performed on the same extracts used for H₂O₂ detection. The considered time points were then 24 h, 48 h, and 96 h for both shoots and roots. In general, 44 compounds belonging to different polyphenol classes were identified in both NNMF and GMF samples, including 8 flavanols (Figure 4 compounds 7, 11, 16, 19, 26, 34, 41, and 45), 13 flavonols (compounds 10, 13, 14, 15, 18, 20, 22, 24, 29, 33, 39, 42, and 43), 10 isoflavanones (compounds 3, 5, 6, 9, 21, 28, 31, 35, 36, and 40), and 6 O-methylated flavonols (compounds 12, 17, 30, 32, 44, and 23) (see Supplementary Table S5 for quantitative variation and Figure 4 for chemical structures).

Table 8 shows the content of the total identified polyphenols expressed as $\mu\text{g g}^{-1}$ FW, along with the NNMF/GMF ratio. In general, at 96 h, both roots and shoots showed a total polyphenol content that was always lower under NNMF than GMF. From 24 h to 48 h, the shoots polyphenol content showed a decreasing trend with time, whereas in roots the highest value was found at 48 h (Table 8).

Table 8. Time-course analysis of total polyphenol contents in *Arabidopsis thaliana* under GMF and NNMF. Values are expressed as $\mu\text{g g}^{-1}$ FW or fold change (NNMF/GMF). Within the same column, letters indicate statistical difference ($p < 0.05$) among shoots (lowercase letters) or roots (uppercase letters), as measured by one-way ANOVA followed by Tukey's test. p value refers to the statistical difference in polyphenol content between plants grown under GMF or NNMF with the same sampling timing. For further statistical information see Supplementary Table S6.

Organ	Timing	GMF $\mu\text{g g}^{-1}$ FW	NNMF $\mu\text{g g}^{-1}$ FW	NNMF/GMF	p Value
Shoots	24 h	260.753 (6.005) ^b	707.880 (20.365) ^b	2.714 (0.076)	<0.001
	48 h	557.101 (20.729) ^a	1003.704 (22.784) ^a	1.801 (0.069)	<0.001
	96 h	204.548 (3.458) ^c	125.134 (3.532) ^c	0.611 (0.018)	<0.001
Roots	24 h	109.149 (9.445) ^{AB}	210.005 (3.922) ^B	1.924 (0.025)	<0.001
	48 h	85.917 (6.197) ^B	264.412 (7.945) ^A	3.077 (0.061)	<0.001
	96 h	122.059 (9.173) ^A	87.315 (1.791) ^C	0.715 (0.024)	<0.001

In order to evaluate whether NNMF could affect the content of specific polyphenols, raw data obtained from HPLC-DAD-MS/MS analyses (see Supplementary Table S5) were used to calculate the NNMF/GMF ratio (Table 9). Data indicate that NNMF differently modulates the content of polyphenols, not only within the two organs, but also with time.

Table 9. Fold change values of NNMF vs. GMF polyphenols in *Arabidopsis thaliana* time-course experiments from Supplementary Table S4. Fold change values are expressed along with standard deviation and calculated from the quantitative data of Supplementary Table S5.

#	Compound(s)	Roots			Shoots		
		24 h	48 h	96 h	24 h	48 h	96 h
1	Daidzein-galactoside	1.392 (0.026)	2.23 (0.083)	1.542 (0.032)	8.542 (0.149)	9.238 (0.195)	0.403 (0.007)
2	Genistein-galactoside				0.656 (0.02)	0.325 (0.009)	0.785 (0.011)
3	Dihydrogenistein-galactoside				11.568 (0.164)	0.127 (0.003)	0.874 (0.026)
4	Genistein-glucoside				1.424 (0.032)	0.746 (0.013)	1.587 (0.041)
5	Dihydrogenistein-glucoside				3.611 (0.056)	1.443 (0.051)	0.885 (0.025)

Table 9. Cont.

#	Compound(s)	Roots			Shoots		
		24 h	48 h	96 h	24 h	48 h	96 h
6	Dihydrogenistein-glucuronide	3.251 (0.125)	4.071 (0.065)	5.032 (0.127)	0.712 (0.013)	6.491 (0.108)	0.715 (0.027)
7	Dihydrokaempferol-glucoside				1.371 (0.053)	1.507 (0.056)	0.845 (0.019)
8	Daidzein-glucoside	1.353 (0.03)	2.986 (0.063)	0.624 (0.024)	2.134 (0.034)	3.024 (0.1)	0.664 (0.008)
9	Dihydromyricetin-diglucoside	2.214 (0.042)	4.495 (0.125)	0.475 (0.013)	3.111 (0.045)	1.452 (0.03)	0.614 (0.016)
10	Quercetin-rutinoside	2.232 (0.088)	1.087 (0.027)	0.368 (0.004)	1.219 (0.046)	1.902 (0.043)	0.272 (0.006)
11	Dihydroquercetin-rutinoside	1.883 (0.042)	0.316 (0.008)	4.69 (0.145)	0.763 (0.025)	9.222 (0.176)	0.236 (0.007)
12	Dihydrohesperetin-neohesperidoside				5.245 (0.199)	1.489 (0.048)	0.27 (0.007)
13	Kaempferol-rutinoside	6.88 (0.114)	2.932 (0.108)	0.996 (0.025)		0.763 (0.015)	1.054 (0.033)
14	Quercetin-sambubioside	2.126 (0.075)	4.211 (0.08)	0.826 (0.03)	4.615 (0.092)	2.284 (0.04)	0.489 (0.018)
15	Quercetin-dirhamnopyranoside	7.846 (0.192)	2.903 (0.101)	0.973 (0.031)	0.933 (0.017)	7.443 (0.129)	0.692 (0.007)
16	Dihydroquercetin-sambubioside	3.19 (0.099)	5.405 (0.132)	0.338 (0.004)	3.303 (0.036)	3.638 (0.104)	0.407 (0.012)
17	Isorhamnetin-rutinoside	1.538 (0.05)	3.06 (0.1)	0.533 (0.016)	2.299 (0.074)	2.38 (0.081)	0.404 (0.014)
18	Myricetin-rutinoside	1.23 (0.022)	3.246 (0.111)	1.072 (0.035)	4.066 (0.09)	2.209 (0.076)	0.374 (0.007)
19	Dihydroquercetin-galactoside	1.178 (0.042)	3.57 (0.103)	0.597 (0.016)	3.811 (0.072)	1.367 (0.034)	1.171 (0.038)
20	Kaempferol-sambubioside				3.914 (0.11)	2.425 (0.073)	0.651 (0.019)
21	Dihydromyricetin-sambubioside				1.423 (0.017)	6.134 (0.215)	0.671 (0.015)
22	Myricetin-diglucoside				1.206 (0.02)	2.128 (0.071)	3.415 (0.049)
23	Isorhamnetin-sambubioside	4.069 (0.138)	5.173 (0.067)	1.371 (0.019)	3.297 (0.099)	2.368 (0.076)	0.571 (0.014)
24	Quercetin-rhamnoside	1.699 (0.019)	5.881 (0.157)	0.121 (0.004)	1.088 (0.023)	2.791 (0.062)	1.139 (0.018)
25	Daidzein-glucuronide	1.889 (0.069)	4.057 (0.113)	0.62 (0.024)	0.373 (0.008)	0.35 (0.01)	0.741 (0.029)
26	Dihydroquercetin-glucoside	2.536 (0.078)	5.348 (0.129)	1.658 (0.052)	5.106 (0.178)	0.168 (0.006)	1.199 (0.016)
27	Unknown	1.862 (0.068)	2.412 (0.072)	0.257 (0.006)	0.27 (0.005)	0.264 (0.004)	5.933 (0.105)
28	Dihydromyricetin-galactoside	1.952 (0.046)	2.301 (0.062)	0.248 (0.007)	0.626 (0.017)	0.206 (0.007)	0.574 (0.016)
29	Quercetin-galactoside	1.933 (0.021)	6.731 (0.21)	0.578 (0.008)	3.349 (0.044)	0.41 (0.004)	0.895 (0.017)
30	Isorhamnetin-galactoside	8.576 (0.097)	4.028 (0.048)	0.545 (0.016)			
31	Dihydromyricetin-rutinoside				1.871 (0.055)	1.216 (0.031)	1.017 (0.015)
32	Isorhamnetin-glucoside	0.621 (0.01)	3.002 (0.077)	0.638 (0.011)			
33	Quercetin-glucoside	0.582 (0.013)	9.052 (0.114)	0.443 (0.009)	0.224 (0.004)	0.737 (0.02)	0.562 (0.02)
34	Dihydroquercetin-diglucoside				0.989 (0.011)	2.824 (0.102)	0.703 (0.017)
35	Dihydromyricetin-glucoside	1.74 (0.038)	1.481 (0.017)	2.263 (0.079)	3.228 (0.082)	1.366 (0.036)	1.8 (0.031)
36	Dihydromyricetin-rhamnoside	1.703 (0.052)	3.06 (0.082)	0.917 (0.016)	4.886 (0.103)	1.459 (0.039)	1.984 (0.041)
37	Genistein	1.418 (0.027)	2.792 (0.083)	1.166 (0.033)	4.146 (0.148)	1.532 (0.028)	1.176 (0.019)
38	Daidzein	8.564 (0.294)	2.658 (0.083)	0.795 (0.021)	2.074 (0.036)	3.164 (0.119)	0.481 (0.015)
39	Kaempferol				4.634 (0.121)	5.079 (0.089)	0.213 (0.004)
40	Dihydrogenistein	4.147 (0.153)	6.492 (0.105)	0.485 (0.018)	4.153 (0.085)	1.625 (0.046)	0.452 (0.011)
41	Dihydrokaempferol				7.355 (0.087)	13.806 (0.438)	5.086 (0.106)
42	Quercetin	1.26 (0.031)	1.316 (0.014)	0.524 (0.011)	4.703 (0.163)	9.87 (0.229)	1.44 (0.022)
43	Myricetin	1.658 (0.021)	7.513 (0.157)	0.831 (0.018)	4.685 (0.147)	1.552 (0.019)	0.494 (0.016)
44	Isorhamnetin	1.726 (0.026)	0.022 (0)	0.799 (0.022)	4.673 (0.062)	1.612 (0.027)	0.452 (0.004)
45	Dihydroquercetin				3.936 (0.147)	2.938 (0.107)	0.616 (0.013)

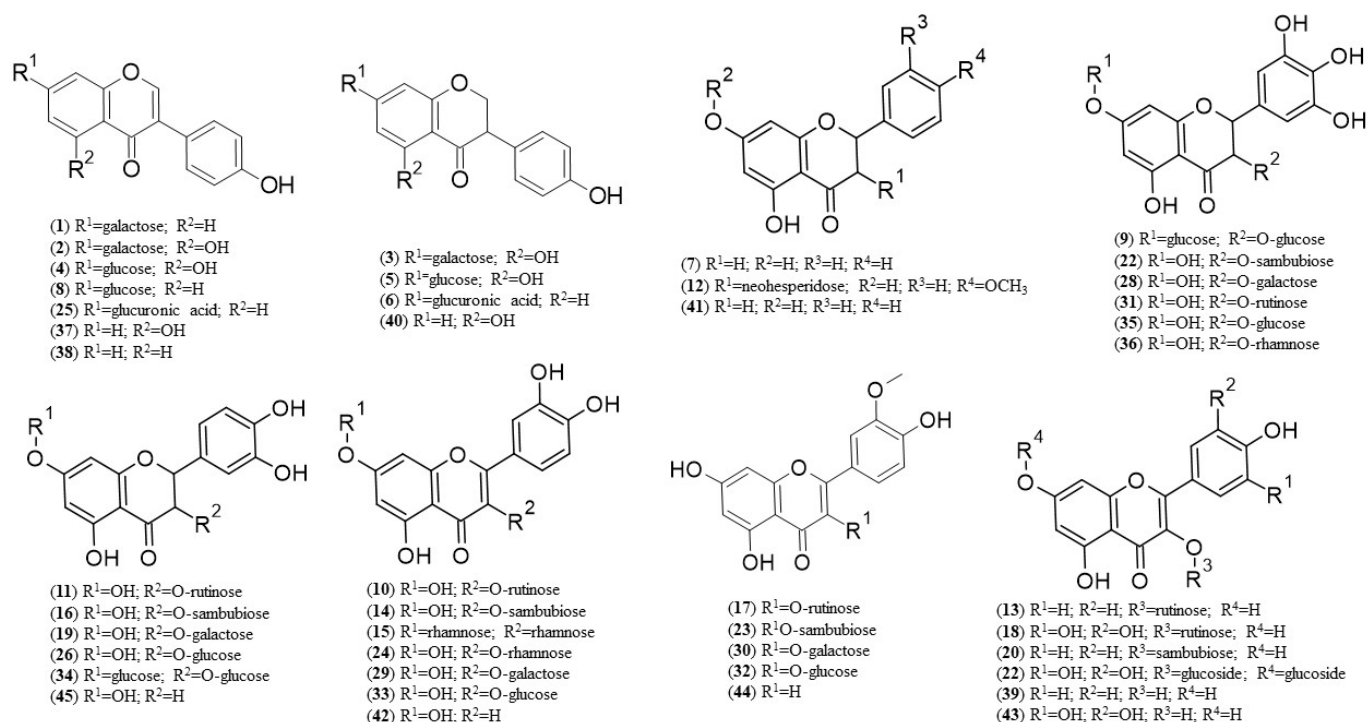


Figure 4. Chemical structure of polyphenolic compounds identified in *Arabidopsis thaliana* roots and shoots grown under GMF and NNMF conditions. Formulae numbers refer to the compounds cited in the main text and in Table 9.

In roots, plants grown for 24 h under NNMF conditions showed a general increase in polyphenols, when compared to GMF, with the sole exception for isorhamnetin glucoside (32) and quercetin glucoside (33) (Table 9). At 48 h, the production of polyphenols was even higher in NNMF, with the exception for dihydroquercetin-rutinoside (11) and isorhamnetin (44), which were reduced. At 96 h, root polyphenols showed a reversed trend and only daidzein-galactoside (1), dihydrogenistein-glucuronide (6), isorhamnetin-sambubioside (23), dihydroquercetin-glucoside (26), dihydromyricetin-glucoside (35) and genistein (37) remained upregulated; interestingly, dihydroquercetin-rutinoside (11), which was reduced at 24 h, increased at 96 h (Table 9).

At all times, shoots contained 14 polyphenols that were not found in roots: genistein-galactoside (2), dihydrogenistein-galactoside (3), genistein-glucoside (4), dihydrogenistein-glucoside (5), dihydrokaempferol-glucoside (7), dihydrohesperetin-neohesperidoside (12), kaempferol-sambubioside (20), dihydromyricetin-sambubioside (28), myricetin-diglucoside (22), dihydromyricetin-rutinoside (31), dihydroquercetin-diglucoside (34), kaempferol (39), dihydrokaempferol (41) and dihydroquercetin (45). However, shoots lacked isorhamnetin-galactoside (30) and isorhamnetin-glucoside (32) at all times and kaempferol-rutinoside (13) at 24 h, with respect to roots. At 24 h, most of the polyphenols were upregulated in NNMF, with particular reference to dihydrogenistein-galactoside (3); however, a significant reduction was found for genistein-galactoside (2), dihydrogenistein-glucuronide (6), dihydroquercetin-rutinoside (11), daidzein-glucuronide (25), dihydromyricetin-galactoside (28), quercetin-glucoside (33), and an unknown polyphenol (27). Upregulation was also found at 48 h NNMF treated plants for most of the identified compounds, with a strong increase of dihydrokaempferol (41); whereas dihydrogenistein-galactoside (3) and dihydroquercetin-glucoside (26) were severely reduced. Finally, at 96 h a general reduction of most of the shoot polyphenols was observed in NNMF plants, with the sole exception for myricetin-diglucoside (22), dihydrokaempferol (41), and an unknown polyphenol (27) that showed a higher induction with respect to GMF plants (Table 9).

In order to evaluate whether the observed differences in the root and shoot polyphenols could match the DEGs, we extracted from the general gene microarray analysis those

genes that were involved in flavonoid biosynthesis (see Supplementary Table S7). Data were then used, along with those reported in Table 9, to generate heatmaps coupled with hierarchical cluster analysis (Figure 5).

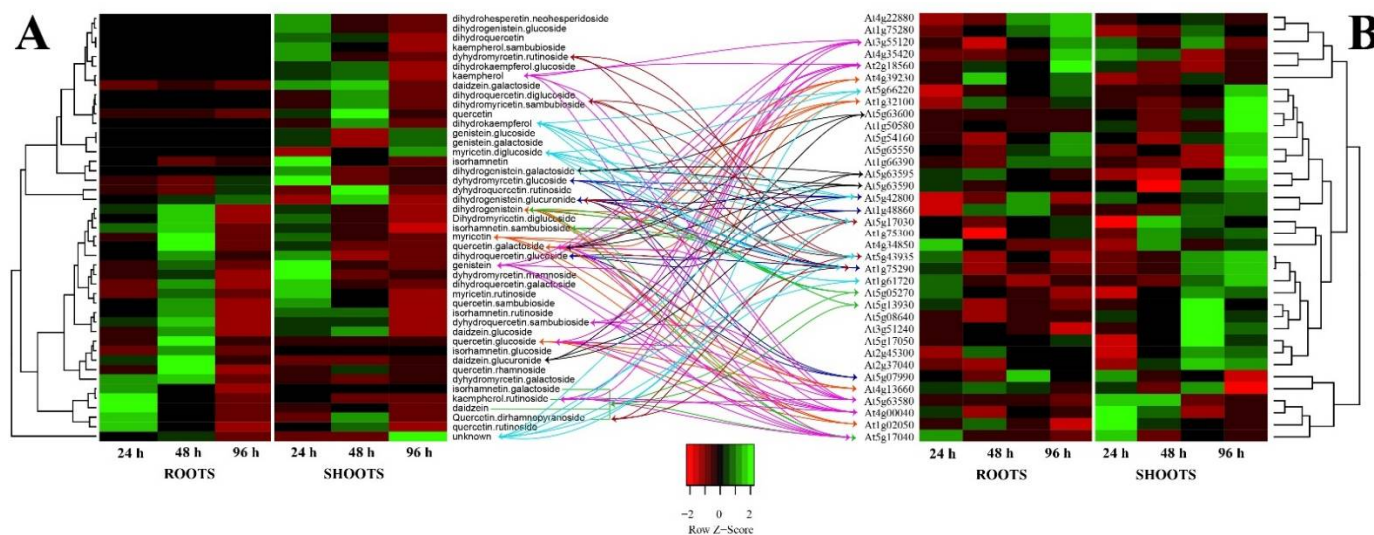


Figure 5. Direct comparison of heatmaps of polyphenols fold change obtained from data of Table 9 (Panel (A)) and fold change of selected genes involved in polyphenols' metabolisms obtained from Supplementary Table S7 (Panel (B)). The heatmap was generated by using a single linkage clustering method and a Pearson distance measuring method. Downregulated genes are marked in red-shaded colors, whereas upregulation is evidenced by different shades of green. See text for arrow color specifications.

A direct comparison between polyphenol quantity (Figure 5A) and DEGs expressing polyphenol metabolism (Figure 5B) shows a gene upregulation of *chalcone synthase* (*At5g13930*), *chalcone isomerase* (*At5g05270*) and *UDP-glucosyl transferase* (*At5g17040*) in roots at 4 h, that preceded the reduced biosynthesis of isorhamnetin-galactoside (30), daidzein (38), quercetin-dirhamnopyranoside (15), kaempferol-rutinoside (13), dihydrogenistein (40), and isorhamnetin-sambubioside (23) that were detected at 24 h (Figure 5 green arrows). At 24 h, root upregulation of *phenylcoumaran benzylic ether reductase 1* (*At4g39230*), *pinoresinol reductase 1* (*At1g32100*), *pinoresinol reductase 2* (*At4g13660*), and *polyketide synthase A* (*At1g02050*) preceded the biosynthesis of several polyphenols at 48 h, with particular reference to quercetin-glucoside (33), myricetin (43), quercetin-galactoside (29), and dihydrogenistein (40) (Figure 5 orange arrows). Finally, the root DEGs at 48 h were characterized by general downregulation, which matched with the low amount of polyphenols detected at 96 h (Figure 4A), with the exception for *DFR* (*At5g42800*), *EPSPS* (*At1g48860*), *CYP75B1* (*At5g07990*), and a putative *isoflavone reductase* (*At1g75290*), which upregulation-matched with the higher levels of dihydrogenistein-glucuronide (6), dihydroquercetin-glucoside (26), and dihydromyricetin-glucoside (35) (Figure 5 blue arrows).

With regards shoots, the gene upregulation of *chalcone synthase* (*At4g00040* and *At1g02050*), *chalcone isomerase* (*At3g55120*), *flavonol synthase* (*At5g63580*), and *UDP-glucosyl transferase* (*At5g17040* and *At2g18560*) preceded the synthesis of the most polyphenols detected at 24 h, including genistein (37), quercetin-sambubioside (14), quercetin-glucoside (33), quercetin-galactoside (29), kaempferol (39), and kaempferol-rutinoside (13) (Figure 5 purple arrows). The shoot DEGs at 24 h were characterized by a downregulation of several flavonol synthases including *FLS3* (*At5g63590*), *FLS4* (*At5g63595*), and *FLS5* (*At5g63600*) that matched with the reduced production of dihydrogenistein-galactoside (3), daidzein-glucuronide (25), and quercetin-galactoside (29) at 48 h (Figure 3 black arrows). The upregulation of *UDP-glucosyl transferase* (*At5g17030*), *FLS6* (*At5g43935*), and a putative *isoflavone reductase* (*At1g75290*) at 24 h matched with the increased amount, among

others, of dihydrogenistein-glucuronide (6), dihydroquercetin-rutinoside (11), quercetin-dirhamnopyranoside (15), dihydromyricetin-sambubioside (21), and dihydrokaempferol (41) (Figure 3 maroon arrows). Finally, the shoot DEGs at 48 h were characterized by the upregulation of an isoflavone reductase (At1g75290), FLS6 (At5g43935), chalcone and stilbene synthase (At5g66220), UDP-glucosyl transferase (At5g17030), DFR (At5g42800), and BAN (At1g61720), that matched the higher production of myricetin-diglucoside (22), an unknown polyphenol (27), and dihydrokaempferol (41) at 96 h (Figure 5 light blue arrow).

4. Discussion

MF variations induce in plants a typical abiotic stress response, with differential expression of several genes, including DEGs coding for responses to oxidative stress [20]. ROS comprise a wide array of oxygen-derived compounds with varying rates of reactivity and may be produced by either endogenous or exogenous stimulation [30]. H₂O₂, a non-radical ROS, is mainly produced by the plasma membrane-located NADPH oxidase (also known as the respiratory burst oxidase homologs, RBOHs) that produces the superoxide anion, which in turn is reduced by superoxide dismutase (SOD) to H₂O₂ [31]. The latter is detoxified to water by a number of scavenging enzymes, including several peroxidases [32]. Despite the disrupting effects, the timely and appropriate production of H₂O₂ can act as a signal for plant responses to environmental stresses [33] and our data indicate that in normal GMF conditions ROS are produced. Evidence indicates that reduction in GMF affects cellular ROS levels and alters their normal signaling roles in regulating the diverse cellular physiological processes [34]. The effect of both static MF and extremely low-frequency MF have been demonstrated to exert an effect on ROS production [3,4,21] and our data provide evidence on the relationship between H₂O₂ production and metabolomics/transcriptomics of ROS scavenging systems under NNMF conditions.

Our results show that reduction of GMF to NNMF causes root/shoot expression of several DEGs coding for enzymes involved in oxidative reactions and confirm the hormetic behavior in time-course experiments. We identified several DEGs in the two analyzed organs (roots and shoots). We noted the constant upregulation of shoot *monoamine-oxidase A repressor R1 protein* (At1g67270), which is always downregulated in roots. Because monoamine oxidase A (MAO-A) degrades biogenic amines producing reactive oxygen, the inhibition of MAO-A promoter by the upregulation of this zinc-finger transcription factor may result in the reduction not only of MAO enzymatic activity, but also in the concomitant decrease of ROS production in the shoots [35]. A common root and shoot upregulation was found for several oxygenases. Among these, *AERO2* is known for its involvement in the oxidative protein folding in the endoplasmic reticulum [36], whereas *GULLO1*, which takes also part as *AERO2* of the secretory pathway, is known to code for a D-arabinono-1,4-lactone oxidase and is involved in the production of L-ascorbic acid, an important antioxidant and redox molecule [37]. Other common DEGs were *GOXL5*, a galactose oxidase that is involved in pectin crosslinking through modification of galactose side chain [38], *OGO3*, an oligogalacturonide oxidase plant berberine bridge enzyme-like oligosaccharide oxidase that oxidizes oligogalacturonide and cellodextrin [39], and several 2-oxoglutarates (2OG) and Fe(II)-dependent oxygenases, which are important oxidizing biological catalysts whose activity is usually increased by the contribution of catalase and ascorbate [40]. Interestingly, a consistent downregulation was found for a plant cysteine oxidase (*PCO3*), which is involved in the N-end rule pathway-mediated proteolysis for degradation via the 26S proteasome [41].

The reduction of GMF to NNMF also decreased the *A. thaliana* H₂O₂ production both in roots and shoots. This effect appears to be related to a modulation of DEGs coding for enzymes involved in ROS scavenging as well as the increased production of polyphenols with antioxidant properties. As already observed in our previous studies [20], the differential gene expression between organs suggests the regulation of overlapping sets of stress-responsive genes.

Both NNMF and GMF plants show developmental changes in ROS production. NNMF exposed plants show an increasing trend in ROS production, although these values are always lower when compared to GMF plants (see Table 7). However, this increase was associated to the upregulation of genes encoding for enzymes involved in ROS production, such as *RBOHH*, *RBOHJ*, *RBOHG*, *SOD1*, *SOD2*, and *CCS*. *RBOHH* and *RBOHJ* are regulated by cytosolic calcium and protein phosphorylation, and their H_2O_2 production was found to dampen growth rate oscillations [42]. Previous studies have shown that NNMF modulates the ion homeostasis and affects calcium levels [43]. Although no data are available on *RBOHG* function, some *RBOHs* have been found to activate a ROS signaling that induces polyphenol biosynthesis genes, thus enabling their accumulation in plants [44]. *SOD1* is cytosolic and *SOD2* is attached to thylakoid membranes where *PSI* is located and are two isoforms of *SOD* expressed in photosynthetic tissues [45]. Overexpression of *SOD* genes increases the tolerance to abiotic stresses in many plant species, including *A. thaliana* [46]. *CCS*, or Cu chaperone for *SOD* (*At1g12520*), is localized to the chloroplast, expressed in roots and shoots, and is required to insert Cu and activate *SOD* [47]. *SOD1* activation in the cytoplasm involves both a *CCS*-dependent and -independent pathways, whereas *SOD2* dismutates the superoxide anion produced by *PSI*, resulting in the formation H_2O_2 , and its activation depends totally on *CCS* [48].

We also noticed that the reduction in H_2O_2 of NNMF plants was associated with the upregulation of several genes coding for ROS scavengers, including several peroxidases, some of which (*PER6*, *PER28*, *PER36*, and *At3g42570*) were upregulated at all sampling times and in both organs. These class III peroxidases (E.C.1.11.1.7) are involved in oxidation reactions that use H_2O_2 as an electron acceptor and several substrates as electron donors [49]. *PER6*, *PER28*, and the peroxidase coded by *At3g42570* are present in all organs [50], whereas *PER36* is extracellular and mainly located in internodes and developing seeds. *PER6* loosens cell walls, apparently contributing to disruption of polysaccharide bonds, which is required for cell elongation during growth [49].

There was a clear relationship between H_2O_2 production and the presence of antioxidant biomolecules. Even in this case, polyphenols were observed to change their content during development in both NNMF- and GMF-exposed plants. The increasing trend of H_2O_2 production in NNMF-exposed plants was associated with a progressive reduction of polyphenols (Tables 7 and 8). Since antioxidant polyphenols scavenge free radicals and repair damaged cells, they are active in protecting plant cells from oxidative stress [51]. At 24 h of NNMF exposure, in both roots and shoots, the high content of polyphenols was dominated by flavonols, isoflavones, and isoflavanones. Interestingly, the high production of the isoflavonoids daidzein (38) and dihydrogenistein (40) was preceded by the upregulation of an isoflavone reductase (*At1g75290*), whereas the higher contents of the flavonols dihydroquercetin-glucoside (26), quercetin-sambubioside (14), dihydroquercetin-sambubioside (16), and isorhamnetin-sambubioside (23) were preceded by the upregulation of genes involved in flavan-3-ols synthesis (*BAN*) and flavonol biosynthetic process (*FLS6*). The formation of flavonols depends on flavonol synthase (*FLS*); in *A. thaliana*, only *FLS1* appears to be functionally expressed and *FLS6* has been identified as pseudogene because of its considerably truncated C-termini [52]. Nevertheless, some *FLS* might retain some activity in flavonol metabolism [53].

Low levels of polyphenols in both roots and shoots at 96 h NNMF exposure were associated to a general drop in flavonol biosynthesis, which corresponded to the downregulation of *FLS2* and *DRL1*. *FLS2* is present in small and medium-size leaves and its expression has been reported to be constitutive but much lower than for *FLS1* [54]. *DRL1* is essential for pollen development and male fertility in *A. thaliana* and encodes for a dihydroflavonol 4-reductase-like1 protein, which is an NADPH-dependent enzyme converting dihydroflavonols to their corresponding leucoanthocyanidins [55]. Among polyphenols, both roots and shoots of NNMF plants show a significant drop of quercetin-rutinoside (10), isorhamnetin-rutinoside (17), and dihydromyricetin-galactoside (28).

5. Conclusions

Either static or oscillating weak magnetic fields with a higher intensity than the GMF have been reported to induce oxidative stress [6,56], suggesting the involvement of the radical pair mechanisms [15] with the contribution of both mitochondria [57] and chloroplasts [58]. The primary effect of a MF with respect to cryptochrome function has been postulated to be the modulation of ROS [19,59]. This mechanism perfectly predicts an effect on cellular ROS signaling pathways; therefore, this hypothesis explains the ROS-related modulation of gene expression in response to reduced MFs as observed in our work.

Typically, variations in MF-dependent ROS production are accompanied by variations in antioxidants [60]. From a transcriptomic point of view, we identified different classes of “oxidases” including RBOHs and several peroxidases that play hormetic roles in both root and shoot MF-dependent oxidative stress. Our results also indicate that polyphenols represent a contributing factor involved in the antioxidant response to varying MFs and confirm previous studies indicating the modulation of flavonoids and other polyphenols by MF [61–64]. We identified some key isoflavonoids like daidzein (38) and dihydrogenistein (40), and flavonols including dihydroquercetin-glucoside (26), quercetin-sambubioside (14), dihydroquercetin-sambubioside (16), and isorhamnetin-sambubioside (23), along with the regulation of the associated genes such as isoflavone reductase (*At1g75290*) and some flavonol synthases that deserve further studies.

In conclusion, our results indicate that the GMF induces a basic oxidative stress, which is characterized by the downregulation of genes coding for scavenging enzymes and the upregulation of genes that code for enzymes that contribute to ROS production. We hypothesize that this condition generates a mild oxidative stress condition that plants evolved in a GMF environment. Changes in MF induce in plants changes in the redox status, indicating a functional role of plant magnetoperception in response to stress. Therefore, we believe that MF variations can be considered an abiotic stress factor, triggered by a still-unknown mechanism of magnetic induction [18] that is first evidenced by a plant's alteration of the redox status.

Supplementary Materials: The following supporting information can be downloaded at: <https://www.mdpi.com/article/10.3390/biom12121824/s1>, Supplementary Dataset S1: gene expression changes, statistical analysis and fold change volcano plots for all time points assessed; Table S1: list of primers; Table S2: genes explained a fold change value >2 at almost all timing point points; Table S3: HSD post-test of H₂O₂ content; Table S4: genes coding for ROS-scavenging enzymes selected from Supplementary Table S2; Table S5: HPLC-DAD-MS/MS quantification of polyphenols in *A. thaliana* grown under GMF and NNMF conditions; Table S6: HSD post-test of polyphenol content; Table S7: genes selected for their involvement in polyphenol metabolism.

Author Contributions: Conceptualization, M.E.M.; methodology, M.E.M., A.S.P. and G.M.; software, M.E.M., A.S.P. and G.M.; validation, M.E.M., A.S.P. and G.M.; formal analysis, M.E.M., A.S.P. and G.M.; investigation, M.E.M., A.S.P. and G.M.; resources, M.E.M.; data curation, M.E.M., A.S.P. and G.M.; writing—original draft preparation, M.E.M.; writing—review and editing, M.E.M., A.S.P. and G.M.; project administration, M.E.M.; funding acquisition, M.E.M. All authors have read and agreed to the published version of the manuscript.

Funding: This research was funded by the University of Turin Local research grant MAFM_RILO_22_01 to M.E.M.

Institutional Review Board Statement: Not applicable.

Informed Consent Statement: Not applicable.

Data Availability Statement: Data are available as supplementary tables and further data can be provided upon request.

Conflicts of Interest: The authors declare no conflict of interest.

References

1. Radhakrishnan, R. Magnetic field regulates plant functions, growth and enhances tolerance against environmental stresses. *Physiol. Mol. Biol. Plants* **2019**, *25*, 1107–1119. [[CrossRef](#)]
2. Teixeira da Silva, J.A.; Dobranszki, J. Magnetic fields: How is plant growth and development impacted? *Protoplasma* **2016**, *253*, 231–248. [[CrossRef](#)] [[PubMed](#)]
3. Maffei, M.E. Magnetoreception in plants. In *Bioelectromagnetism. History, Foundations and Applications*; Shoogo, U., Tsukasa, S., Eds.; CRC Press: Boca Raton, FL, USA, 2022; pp. 191–214.
4. Maffei, M.E. Magnetic field effects on plant growth, development, and evolution. *Front. Plant Sci.* **2014**, *5*, 445. [[CrossRef](#)]
5. Xu, C.X.; Wei, S.F.; Lu, Y.; Zhang, Y.X.; Chen, C.F.; Song, T. Removal of the local geomagnetic field affects reproductive growth in arabidopsis. *Bioelectromagnetics* **2013**, *34*, 437–442. [[CrossRef](#)]
6. Zadeh-Haghighi, H.; Simon, C. Magnetic field effects in biology from the perspective of the radical pair mechanism. *J. R. Soc. Interface* **2022**, *19*, 39. [[CrossRef](#)]
7. Guo, J.P.; Wan, H.Y.; Matysik, J.; Wang, X.J. Recent advances in magnetosensing cryptochrome model systems. *Acta Chim. Sin.* **2018**, *76*, 597–604. [[CrossRef](#)]
8. Hore, P.J.; Mouritsen, H. The radical-pair mechanism of magnetoreception. *Annu. Rev. Biophys.* **2016**, *45*, 299–344. [[CrossRef](#)]
9. Castello, P.; Jimenez, P.; Martino, C.F. The role of pulsed electromagnetic fields on the radical pair mechanism. *Bioelectromagnetics* **2021**, *42*, 491–500. [[CrossRef](#)]
10. Pooam, M.; Arthaut, L.D.; Burdick, D.; Link, J.; Martino, C.F.; Ahmad, M. Magnetic sensitivity mediated by the arabidopsis blue-light receptor cryptochrome occurs during flavin reoxidation in the dark. *Planta* **2019**, *249*, 319–332. [[CrossRef](#)]
11. Kornig, A.; Winklhofer, M.; Baumgartner, J.; Gonzalez, T.P.; Fratzl, P.; Faivre, D. Magnetite crystal orientation in magnetosome chains. *Adv. Funct. Mater.* **2014**, *24*, 3926–3932. [[CrossRef](#)]
12. Kempster, R.M.; McCarthy, I.D.; Collin, S.P. Phylogenetic and ecological factors influencing the number and distribution of electroreceptors in elasmobranchs. *J. Fish Biol.* **2012**, *80*, 2055–2088. [[CrossRef](#)] [[PubMed](#)]
13. Qin, S.; Yin, H.; Yang, C.; Dou, Y.; Liu, Z.; Zhang, P.; Yu, H.; Huang, Y.; Feng, J.; Hao, J.; et al. A magnetic protein biocompass. *Nat. Mater.* **2016**, *15*, 217–226. [[CrossRef](#)] [[PubMed](#)]
14. Albaqami, M.; Hammad, M.; Pooam, M.; Procopio, M.; Sameti, M.; Ritz, T.; Ahmad, M.; Martino, C.F. Arabidopsis cryptochrome is responsive to radiofrequency (rf) electromagnetic fields. *Sci. Rep.* **2020**, *10*, 11260. [[CrossRef](#)] [[PubMed](#)]
15. Pooam, M.; Jourdan, N.; El Esawi, M.; Sherrard, R.M.; Ahmad, M. Hek293 cell response to static magnetic fields via the radical pair mechanism may explain therapeutic effects of pulsed electromagnetic fields. *PLoS ONE* **2020**, *15*, e0243038. [[CrossRef](#)]
16. Berteza, C.M.; Narayana, R.; Agliassa, C.; Rodgers, C.T.; Maffei, M.E. Geomagnetic field (gmf) and plant evolution: Investigating the effects of gmf reversal on *Arabidopsis thaliana* development and gene expression. *J. Visual. Exp.* **2015**, *105*, e53286. [[CrossRef](#)]
17. Lohmann, K.J. A candidate magnetoreceptor. *Nat. Mater.* **2016**, *15*, 136–138. [[CrossRef](#)]
18. Parmagnani, A.S.; D’Alessandro, S.; Maffei, M.E. Iron-sulfur complex assembly: Potential players of magnetic induction in plants. *Plant Sci.* **2022**, *325*, 111483. [[CrossRef](#)]
19. Pooam, M.; El-Esawi, M.; Aguida, B.; Ahmad, M. Arabidopsis cryptochrome and quantum biology: New insights for plant science and crop improvement. *J. Plant Biochem. Biotechnol.* **2020**, *29*, 636–651. [[CrossRef](#)]
20. Paponov, I.A.; Fliegmann, J.; Narayana, R.; Maffei, M.E. Differential root and shoot magnetoresponses in *Arabidopsis thaliana*. *Sci. Rep.* **2021**, *11*, 14. [[CrossRef](#)]
21. Wang, H.Z.; Zhang, X. Magnetic fields and reactive oxygen species. *Int. J. Mol. Sci.* **2017**, *18*, 2175. [[CrossRef](#)]
22. Massey, V. Activation of molecular oxygen by flavins and flavoproteins. *J. Biol. Chem.* **1994**, *269*, 22459–22462. [[CrossRef](#)] [[PubMed](#)]
23. Usselman, R.J.; Hill, I.; Singel, D.J.; Martino, C.F. Spin biochemistry modulates reactive oxygen species (ros) production by radio frequency magnetic fields. *PLoS ONE* **2014**, *9*, e93065. [[CrossRef](#)]
24. Murashige, T.; Skoog, F. A revised medium for rapid growth and bioassays with tobacco tissue cultures. *Physiol. Plant* **1962**, *15*, 473–497. [[CrossRef](#)]
25. Agliassa, C.; Narayana, R.; Berteza, C.M.; Rodgers, C.T.; Maffei, M.E. Reduction of the geomagnetic field delays *Arabidopsis thaliana* flowering time through downregulation of flowering-related genes. *Bioelectromagnetics* **2018**, *39*, 361–374. [[CrossRef](#)]
26. Brazma, A.; Hingamp, P.; Quackenbush, J.; Sherlock, G.; Spellman, P.; Stoeckert, C.; Aach, J.; Ansorge, W.; Ball, C.A.; Causton, H.C.; et al. Minimum information about a microarray experiment (miame)—Toward standards for microarray data. *Nat. Genet.* **2001**, *29*, 365–371. [[CrossRef](#)] [[PubMed](#)]
27. Smyth, G.K. Limma: Linear models for microarray data. In *Bioinformatics and Computational Biology Solutions Using R and Bioconductor*; Gentleman, R., Carey, V., Dudoit, S., Irizarry, R., Huber, W., Eds.; Springer: New York, NY, USA, 2005; pp. 397–420.
28. Kotz, S.; Lloyd Johnson, N.; Read, C.B. *Encyclopedia of Statistical Sciences*, 1st ed.; Wiley-Interscience: Hoboken, NJ, USA, 1988; Volume 9.
29. Babicki, S.; Arndt, D.; Marcu, A.; Liang, Y.; Grant, J.R.; Maciejewski, A.; Wishart, D.S. Heatmapper: Web-enabled heat mapping for all. *Nucleic Acids Res.* **2016**, *44*, W147–W153. [[CrossRef](#)]
30. Tretter, V.; Hochreiter, B.; Zach, M.L.; Krenn, K.; Klein, K.U. Understanding cellular redox homeostasis: A challenge for precision medicine. *Int. J. Mol. Sci.* **2022**, *23*, 106. [[CrossRef](#)]

31. Chapman, J.M.; Muhlemann, J.K.; Gayornba, S.R.; Muday, G.K. Rboh-dependent ros synthesis and ros scavenging by plant specialized metabolites to modulate plant development and stress responses. *Chem. Res. Toxicol.* **2019**, *32*, 370–396. [[CrossRef](#)]
32. Rhee, S.G. H₂O₂, a necessary evil for cell signaling. *Science* **2006**, *312*, 1882–1883. [[CrossRef](#)]
33. Chen, Q.H.; Yang, G.W. Signal function studies of ros, especially rboh-dependent ros, in plant growth, development and environmental stress. *J. Plant Growth Regul.* **2020**, *39*, 157–171. [[CrossRef](#)]
34. Zhang, B.F.; Tian, L.X. Reactive oxygen species: Potential regulatory molecules in response to hypomagnetic field exposure. *Bioelectromagnetics* **2020**, *41*, 573–580. [[CrossRef](#)]
35. Ou, X.M.; Chen, K.; Shih, J.C. Monoamine oxidase a and repressor r1 are involved in apoptotic signaling pathway. *Proc. Natl. Acad. Sci. USA* **2006**, *103*, 10923–10928. [[CrossRef](#)] [[PubMed](#)]
36. Fan, F.; Zhang, Y.; Huang, G.; Zhang, Q.; Wang, C.-C.; Wang, L.; Lu, D. Atero1 and atero2 exhibit differences in catalyzing oxidative protein folding in the endoplasmic reticulum. *Plant Physiol.* **2019**, *180*, 2022–2033. [[CrossRef](#)]
37. Maruta, T.; Ichikawa, Y.; Mieda, T.; Takeda, T.; Tamoi, M.; Yabuta, Y.; Ishikawa, T.; Shigeoka, S. The contribution of arabidopsis homologs of l-gulonolactone oxidase to the biosynthesis of ascorbic acid. *Biosci. Biotechnol. Biochem.* **2010**, *74*, 1494–1497. [[CrossRef](#)]
38. Šola, K.; Dean, G.H.; Li, Y.; Lohmann, J.; Movahedan, M.; Gilchrist, E.J.; Adams, K.L.; Haughn, G.W. Expression patterns and functional characterization of arabidopsis galactose oxidase-like genes suggest specialized roles for galactose oxidases in plants. *Plant Cell Physiol.* **2021**, *62*, 1927–1943. [[CrossRef](#)]
39. Scortica, A.; Giovannoni, M.; Scafati, V.; Angelucci, F.; Cervone, F.; De Lorenzo, G.; Benedetti, M.; Mattei, B. Berberine bridge enzyme-like oligosaccharide oxidases act as enzymatic transducers between microbial glycoside hydrolases and plant peroxidases. *Mol. Plant-Microbe Interact.* **2022**, *35*, 881–886. [[CrossRef](#)]
40. Farrow, S.C.; Facchini, P.J. Functional diversity of 2-oxoglutarate/fe(ii)-dependent dioxygenases in plant metabolism. *Front. Plant Sci.* **2014**, *5*, 524. [[CrossRef](#)]
41. Weits, D.A.; Giuntoli, B.; Kosmacz, M.; Parlanti, S.; Hubberten, H.M.; Riegler, H.; Hoefgen, R.; Perata, P.; van Dongen, J.T.; Licausi, F. Plant cysteine oxidases control the oxygen-dependent branch of the n-end-rule pathway. *Nat. Commun.* **2014**, *5*, 10. [[CrossRef](#)]
42. Kaya, H.; Nakajima, R.; Iwano, M.; Kanaoka, M.M.; Kimura, S.; Takeda, S.; Kawarazaki, T.; Senzaki, E.; Hamamura, Y.; Higashiyama, T.; et al. Ca²⁺-activated reactive oxygen species production by arabidopsis rboh and rbohj is essential for proper pollen tube tip growth. *Plant Cell* **2014**, *26*, 1069–1080. [[CrossRef](#)] [[PubMed](#)]
43. Narayana, R.; Fliegmann, J.; Paponov, I.; Maffei, M.E. Reduction of geomagnetic field (gmf) to near null magnetic field (nmmf) affects *Arabidopsis thaliana* root mineral nutrition. *Life Sci. Space Res.* **2018**, *19*, 43–50. [[CrossRef](#)]
44. Sun, H.L.; Cao, X.Y.; Wang, X.Y.; Zhang, W.; Li, W.X.; Wang, X.Q.; Liu, S.Q.; Lyu, D.G. Rboh-dependent hydrogen peroxide signaling mediates melatonin-induced anthocyanin biosynthesis in red pear fruit. *Plant Sci.* **2021**, *313*, 11. [[CrossRef](#)]
45. Araki, R.; Mermoud, M.; Yamasaki, H.; Kamiya, T.; Fujiwara, T.; Shikanai, T. Spl7 locally regulates copper-homeostasis-related genes in arabidopsis. *J. Plant Physiol.* **2018**, *224–225*, 137–143. [[CrossRef](#)]
46. Sunkar, R.; Kapoor, A.; Zhu, J.-K. Posttranscriptional induction of two cu/zn superoxide dismutase genes in arabidopsis is mediated by downregulation of mir398 and important for oxidative stress tolerance. *Plant Cell* **2006**, *18*, 2051–2065. [[CrossRef](#)] [[PubMed](#)]
47. Huang, C.-H.; Kuo, W.-Y.; Jinn, T.-L. Models for the mechanism for activating copper-zinc superoxide dismutase in the absence of the ccs cu chaperone in arabidopsis. *Plant Signal. Behav.* **2012**, *7*, 428–430. [[CrossRef](#)]
48. Alscher, R.G.; Erturk, N.; Heath, L.S. Role of superoxide dismutases (sods) in controlling oxidative stress in plants. *J. Exp. Bot.* **2002**, *53*, 1331–1341. [[CrossRef](#)] [[PubMed](#)]
49. Kupriyanova, E.V.; Mamoshina, P.O.; Ezhova, T.A. Evolutionary divergence of *Arabidopsis thaliana* classical peroxidases. *Biochemistry* **2015**, *80*, 1362–1372. [[CrossRef](#)] [[PubMed](#)]
50. Valério, L.; De Meyer, M.; Penel, C.; Dunand, C. Expression analysis of the arabidopsis peroxidase multigenic family. *Phytochemistry* **2004**, *65*, 1331–1342. [[CrossRef](#)] [[PubMed](#)]
51. Shen, N.; Wang, T.F.; Gan, Q.; Liu, S.; Wang, L.; Jin, B. Plant flavonoids: Classification, distribution, biosynthesis, and antioxidant activity. *Food Chem.* **2022**, *383*, 13. [[CrossRef](#)]
52. Stracke, R.; De Vos, R.C.H.; Bartelniewoehner, L.; Ishihara, H.; Sagasser, M.; Martens, S.; Weisshaar, B. Metabolomic and genetic analyses of flavonol synthesis in *Arabidopsis thaliana* support the in vivo involvement of leucoanthocyanidin dioxygenase. *Planta* **2009**, *229*, 427–445. [[CrossRef](#)] [[PubMed](#)]
53. Preuss, A.; Stracke, R.; Weisshaar, B.; Hillebrecht, A.; Matern, U.; Martens, S. *Arabidopsis thaliana* expresses a second functional flavonol synthase. *FEBS Lett.* **2009**, *583*, 1981–1986. [[CrossRef](#)] [[PubMed](#)]
54. Fujita, A.; Goto-Yamamoto, N.; Aramaki, I.; Hashizume, K. Organ-specific transcription of putative flavonol synthase genes of grapevine and effects of plant hormones and shading on flavonol biosynthesis in grape berry skins. *Biosci. Biotechnol. Biochem.* **2006**, *70*, 632–638. [[CrossRef](#)] [[PubMed](#)]
55. Tang, L.K.; Chu, H.; Yip, W.K.; Yeung, E.C.; Lo, C. An anther-specific dihydroflavonol 4-reductase-like gene (drl1) is essential for male fertility in arabidopsis. *New Phytol.* **2009**, *181*, 576–587. [[CrossRef](#)] [[PubMed](#)]
56. Barnes, F.; Greenebaum, B. Role of radical pairs and feedback in weak radio frequency field effects on biological systems. *Environ. Res.* **2018**, *163*, 165–170. [[CrossRef](#)] [[PubMed](#)]

57. Van Huizen, A.V.; Morton, J.M.; Kinsey, L.J.; Von Kannon, D.G.; Saad, M.A.; Birkholz, T.R.; Czajka, J.M.; Cyrus, J.; Barnes, F.S.; Beane, W.S. Weak magnetic fields alter stem cell-mediated growth. *Sci. Adv.* **2019**, *5*, eaau7201. [[CrossRef](#)]
58. Sharma, V.P.; Singh, H.P.; Kohli, R.K.; Batish, D.R. Mobile phone radiation inhibits vigna radiata (mung bean) root growth by inducing oxidative stress. *Sci. Total Environ.* **2009**, *407*, 5543–5547. [[CrossRef](#)] [[PubMed](#)]
59. Kattnig, D.R. Radical-pair-based magnetoreception amplified by radical scavenging: Resilience to spin relaxation. *J. Phys. Chem. B* **2017**, *121*, 10215–10227. [[CrossRef](#)]
60. Cakmak, T.; Cakmak, Z.E.; Dumlupinar, R.; Tekinay, T. Analysis of apoplastic and symplastic antioxidant system in shallot leaves: Impacts of weak static electric and magnetic field. *J. Plant Physiol.* **2012**, *169*, 1066–1073. [[CrossRef](#)]
61. Jouni, F.J.; Abdolmaleki, P.; Ghanati, F. Oxidative stress in broad bean (*Vicia faba* L.) induced by static magnetic field under natural radioactivity. *Mutat. Res. Genet. Toxicol. Environ. Mutagen.* **2012**, *741*, 116–121. [[CrossRef](#)]
62. Hassanpour, H.; Niknam, V. Establishment and assessment of cell suspension cultures of *Matricaria chamomilla* as a possible source of apigenin under static magnetic field. *Plant Cell Tissue Organ Cult.* **2020**, *142*, 583–593. [[CrossRef](#)]
63. Radhakrishnan, R.; Leelapriya, T.; Kumari, B.D.R. Effects of pulsed magnetic field treatment of soybean seeds on calli growth, cell damage, and biochemical changes under salt stress. *Bioelectromagnetics* **2012**, *33*, 670–681. [[CrossRef](#)]
64. Taghizadeh, M.; Nasibi, F.; Kalantari, K.M.; Mohseni-Moghadam, M. Modification of phytochemical production and antioxidant activity of *dracocephalum kotschyi* cells by exposure to static magnetic field and magnetite nanoparticles. *Plant Cell Tissue Organ Cult.* **2021**, *147*, 365–377. [[CrossRef](#)]